

PVDIS baffle studies

R. Holmes*

(Dated: May 17, 2016)

I. INTRODUCTION

The current baffles, referred to as "More1", are based on ones designed for the BaBar magnet. The original set of six baffle plates was augmented with five new plates each of which was created by simply interpolating between two original plates, and the slits were uniformly narrowed to reduce charged pion backgrounds. These baffles have not been optimized for the current geometry and field. This report describes some work done on evaluating the More1 baffle design and modifying it to better match the CLEO field.

II. ZIGZAG BAFFLES

Previous studies have shown the photon background at the LGC is dominated by gammas from π^0 decay interacting in the baffles. These interactions occur predominantly close to one edge of the baffle slits as straight throughs that make it through upstream plates strike corners of downstream plates as sketched schematically on the left side of Fig. 1. Some products of these interactions then make it into the slits with an unimpeded trajectory to the detectors downstream.

As illustrated on the right side of Fig. 1, we can mitigate this background by opening up the widths of the slits in the even-numbered baffle plates. Then some photons that would have interacted close to the slit in these plates instead interact further from the slit in the next downstream plate. Products of these interactions are less likely to escape into the slit before being absorbed. Potentially a reduction in such backgrounds on the order of 50% could be possible with such "zigzag" baffles.

* rsholmes@syr.edu

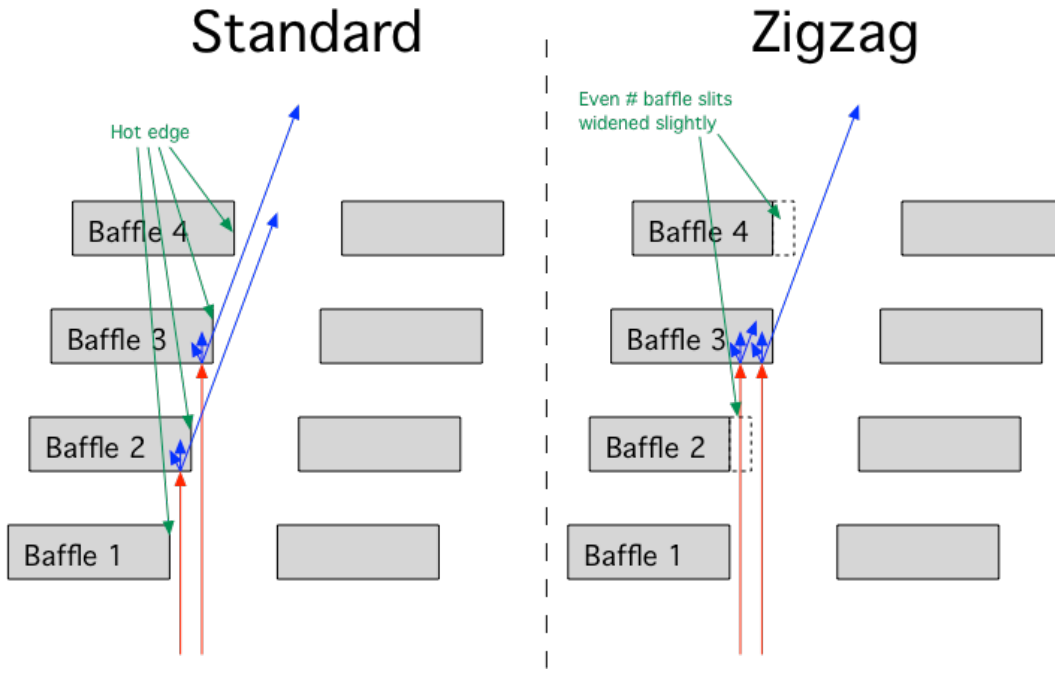


FIG. 1. Left: In the standard More1 baffles, photons from π^0 decay interact primarily in the corners along one edge of the baffle slits. Right: In the zigzag baffles, opening up the slits in the even-numbered plates causes some photons that would have struck near the slit on those plates to instead strike further from the slit on the next plate downstream, reducing background.

This configuration was studied using 6×10^5 events generated by the Wiser π^0 code. The slits in the even-numbered baffles were widened by 1° in the azimuthal angle. There was a 16.3% reduction in the rate of π^0 background photons (from all vertices, in or out of the baffles) with momentum $p > 1$ MeV/c at the third GEM, in front of the LGC, and for $p > 10$ MeV/c, the reduction was 26.5%. See Table I.

Baffle	$p > 1$			$p > 10$		
	standard	zigzag	% diff	standard	zigzag	% diff
1	29740	32529	9.4%	5854	6200	5.9%
2	14784	5124	-65.3%	3461	865	-75.0%
3	15134	18552	22.6%	3444	4084	18.6%
4	13173	2714	-79.4%	3014	361	-88.0%
5	16037	17819	11.1%	3550	3725	4.9%
6	15021	1858	-87.6%	3281	251	-92.3%
7	18780	20968	11.7%	3752	3824	1.9%
8	18952	1464	-92.3%	3619	181	-95.0%
9	23485	29021	23.6%	4071	4337	6.5%
10	28486	2256	-92.1%	4254	215	-94.9%
11	37706	60312	60.0%	5067	6450	27.3%
Total in baffles	231298	192617	-16.7%	43367	30493	-29.7%
Total all z_v	239019	200104	-16.3%	48649	35761	-26.5%

TABLE I. Numbers of photon hits at GEM 3 (at the entrance to the LGC), out of 6×10^5 Wiser π^0 events (uniformly weighted), for standard lead More1 baffles and 1° zigzag lead baffles, and percent differences. Numbers are shown for photons with momentum $p > 1$ MeV/c, and for $p > 10$ MeV/c.

Further studies showed that the size of the zigzag could be reduced from 1° to 0.65° with essentially no change in the background. At this point we hit a wall: further reduction below 0.65° gives rise to significantly higher backgrounds. The slits originally were narrowed to reduce the charged pion background; how much of this background returns

with zigzag baffles? As shown in Table II, the 1° zigzag baffles increase the charged pion background by less than 20% compared to the standard baffles, and the 0.65° zigzag baffles give a less than 10% increase.

Primary	Baffles	π^\pm in GEM 5	% diff
π^+	Standard	1686	
π^+	0.65° Zigzag	1810	7%
π^+	1° Zigzag	2012	19%
π^-	Standard	2692	
π^-	0.65° Zigzag	2867	7%
π^-	1° Zigzag	3051	13%

TABLE II. Charged pion hits at GEM 5 (at the entrance to the EC), out of 6×10^5 Wiser π^+ events and 6×10^5 Wiser π^- events (uniformly weighted), for standard lead More1 baffles, 0.65° zigzag lead baffles, and 1° zigzag lead baffles, and percent differences.

III. MATERIALS

As a baffle material, lead has the advantages of being cheap and dense, with radiation length 0.56 cm and nuclear interaction length 17.6 cm. One disadvantage is its softness. Structural support is needed. Copper is also cheap and has even shorter nuclear interaction length (15.3 cm) though its radiation length is longer (1.4 cm), and is self supporting and easy to machine. Solid tungsten has shorter radiation and nuclear interaction lengths (0.35 cm and 9.9 cm) but is expensive and hard to machine. Tungsten powder mixed with epoxy is easy to mold but is still expensive and has only 60% of the density of solid tungsten, erasing its radiation and nuclear interaction length advantages. Pion and neutron background trigger rates for all these materials are fairly similar, the largest difference being a factor of two better neutron rate in the EC for solid tungsten than for lead.[1]

In the zigzag lead baffles, the largest contributions to the photon background come from interactions in the first baffle, which is exposed to high flux, and the last, which has nothing downstream to block interaction products. Making these two baffles out of solid tungsten would further improve the photon background to a more than 30% reduction relative to the standard baffles (Table III).

Baffle	$p > 1$			$p > 10$		
	standard	zigzag	% diff	standard	zigzag	% diff
1	29740	21101	-29.0%	5854	4285	-26.8%
2	14784	4318	-70.8%	3461	745	-78.5%
3	15134	17925	18.4%	3444	3946	14.6%
4	13173	2495	-81.1%	3014	371	-87.7%
5	16037	17621	9.9%	3550	3689	3.9%
6	15021	1869	-87.6%	3281	288	-91.2%
7	18780	20014	6.6%	3752	3819	1.8%
8	18952	1511	-92.0%	3619	199	-94.5%
9	23485	28402	20.9%	4071	4447	9.2%
10	28486	1912	-93.3%	4254	176	-95.9%
11	37706	40021	6.1%	5067	4206	-17.0%
Total in baffles	231298	157189	-32.0%	43367	26171	-39.7%
Total all z_v	239019	164057	-31.4%	48649	31204	-35.9%

TABLE III. Numbers of photon hits at GEM 3 (at the entrance to the LGC), out of 6×10^5 Wiser π^0 events (uniformly weighted), for standard lead More1 baffles and 1° zigzag baffles (tungsten for plates 1 and 11, lead for plates 2 through 10), and percent differences. Numbers are shown for photons with momentum $p > 1$ MeV/c, and for $p > 10$ MeV/c.

Another possible configuration to consider would be to combine most of the advantages of copper and lead by using baffles which are mainly copper, but with lead pieces lining the slits. For example, for all photon hits in GEM 5 from

electron events (using GEANT to interact 11 GeV electrons in the target), copper baffles give a 15.4% rate increase relative to lead, but lead lined copper baffles (slits lined with lead to a width of 1°) are up only 8.4%; this is further reduced to 1.2% if the last baffle plate is solid lead.

IV. BAFFLE SHAPE

Next I consider the acceptance of the baffles and how it might be optimized.

As seen in Fig. 3.1 of the PVDIS proposal [2], reproduced here as Fig. 2, the useful kinematics region $22^\circ < \theta_p < 35^\circ$ (θ_p is the polar angle of the scattered electron), $x_{Bj} > 0.55$, $W^2 > 4 \text{ GeV}^2$, $Q^2 > 6 \text{ GeV}^2$ defines a stripe in p/θ_p space. Compare to the present baffle acceptance shown in Fig. 3. For this plot I used electrons generated uniformly in

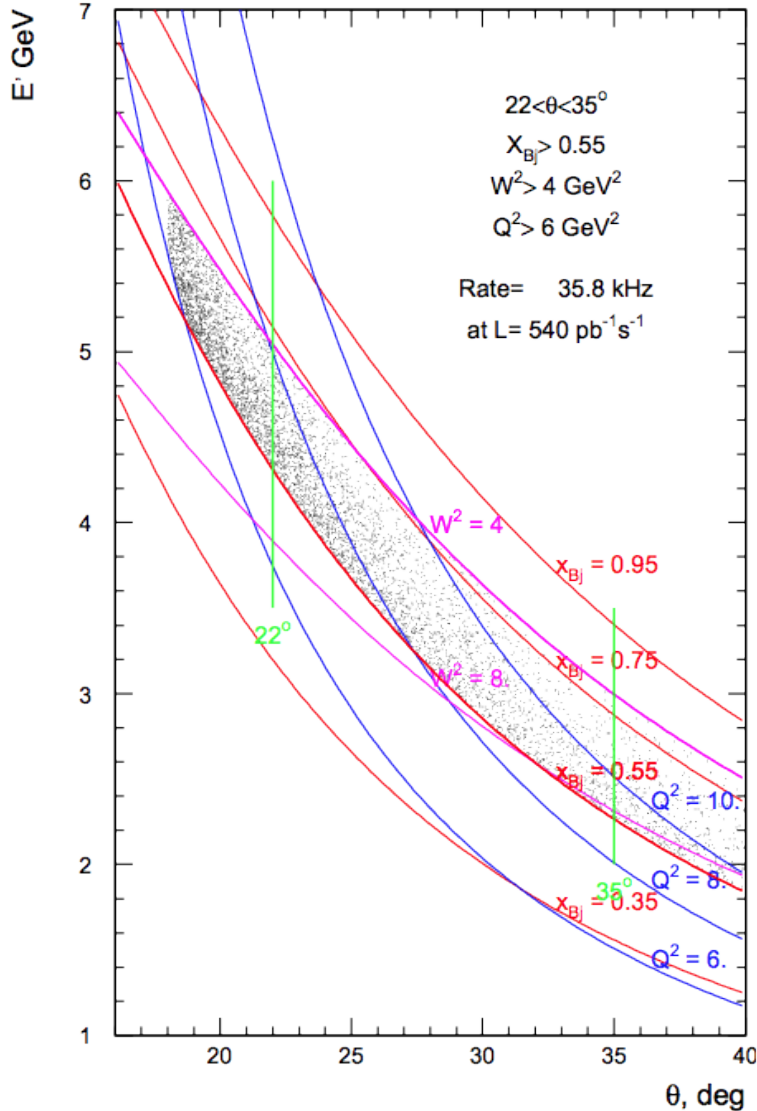


FIG. 2. The useful kinematic range of the scattered electrons is limited by the conditions $x_{Bj} > 0.55$ from the bottom of the plot and $W > 2 \text{ GeV}$ from the top. The DIS events shown on the scatter plot are simulated for the 11 GeV beam. A cut off at $Q^2 > 6 \text{ GeV}^2$ selects the scattered angles of $\theta_p > 18^\circ$.

the range $2 \text{ GeV}/c < p < 6 \text{ GeV}/c$ and $10^\circ < \theta_p < 50^\circ$, from vertices at the target center, and plotted the ratio in each

bin of the number of electrons passing through Kryptonite More1 baffles to the number generated. The acceptance is reasonably well matched to the kinematics of interest.

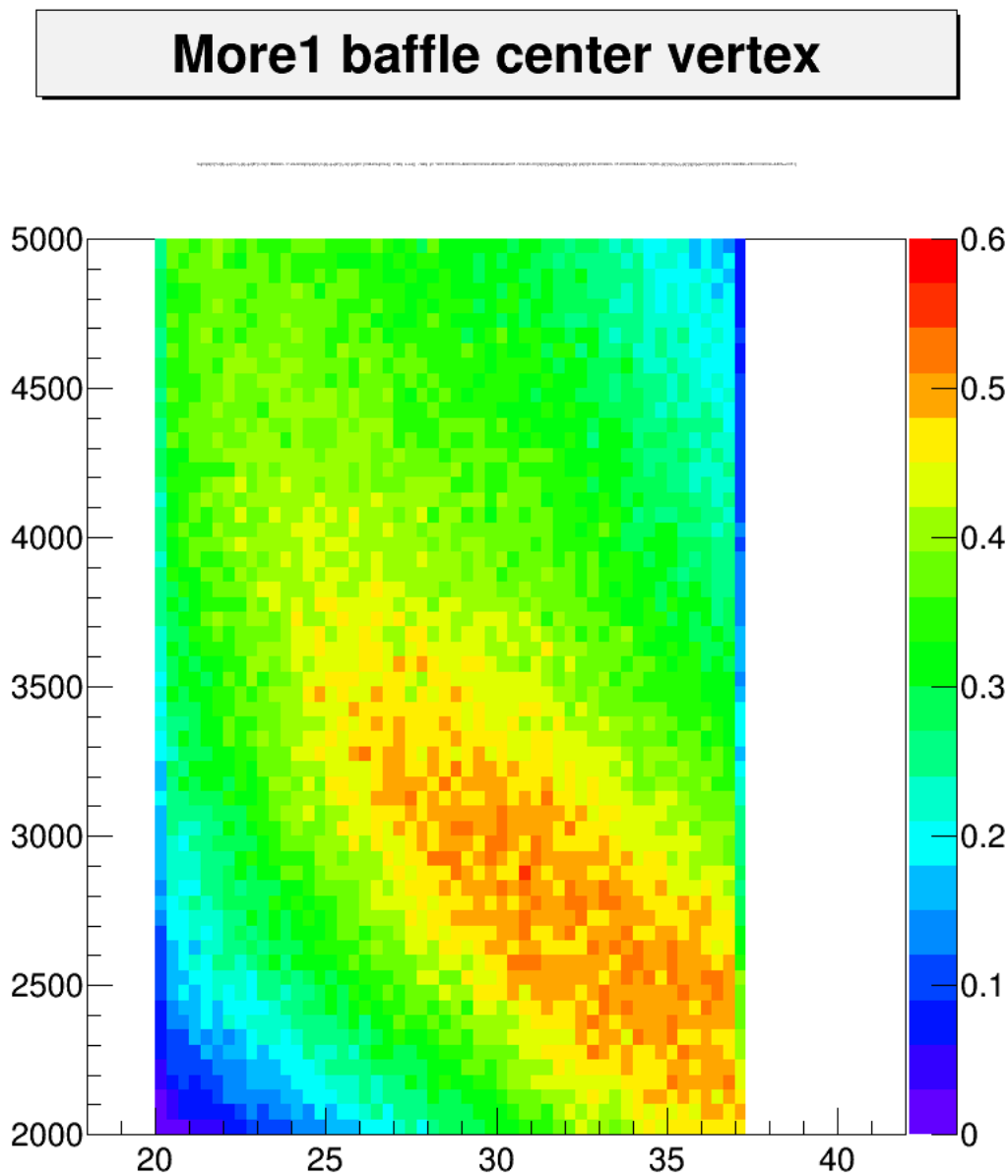


FIG. 3. Acceptance as function of p (MeV/c) vs. θ_p (degrees) for electrons produced at target center and traversing Kryptonite More1 baffles with standard geometry.

Similar acceptance plots are shown in Figs. 4–7 for electrons from vertices at four other positions: the upstream end of the target, halfway between the upstream end and middle, halfway between the middle and downstream end, and the downstream end. There is some loss of acceptance at large angle for upstream vertices, and for vertices near the downstream end the acceptance is nonzero for only a small slice of θ_p at the high end. The latter loss of acceptance is due to electrons striking the inner ring of the upstream baffle plates. As a reminder, the baffle slits do not extend fully to the minimum radius of the baffle plates, so electrons at small radius are blocked regardless of ϕ_p , the azimuthal angle of the scattered electron. Some inner ring may be necessary for mechanical reasons, especially if the baffles are lead, but there is no physics benefit. Figs. 8–9 shows the mid-downstream and downstream vertex acceptances, but

with the inner rings on all plates removed. (A better design probably would be to keep the same baffle plate inner radii, but extend the slits inward.) For the most downstream events, the acceptance is considerably increased.

More1 baffle upstream vertex

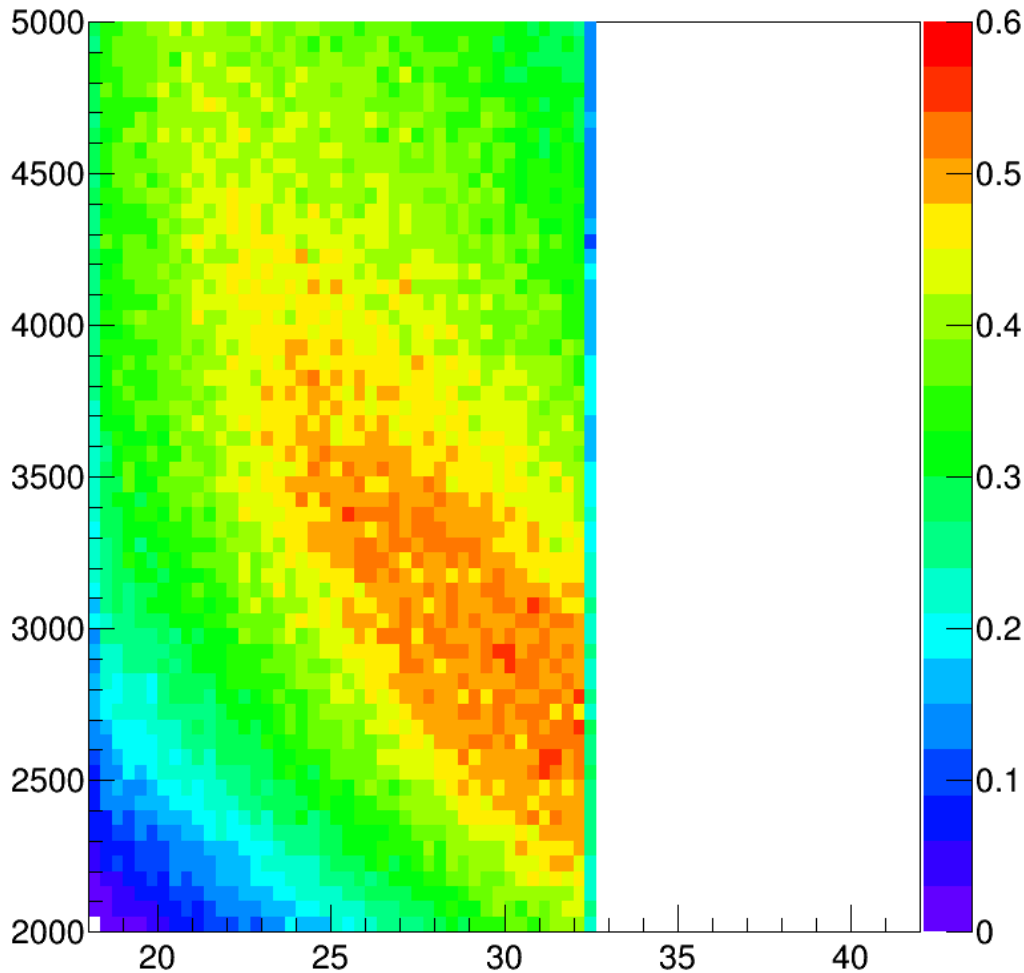


FIG. 4. Acceptance as function of p (MeV/c) vs. θ_p (degrees) for electrons traversing Kryptonite More1 baffles with standard geometry; vertex is at upstream end of target.

Acceptance is affected by the shapes and sizes of the baffle slits. As is evident from Fig. 10, details of the slits are difficult to visualize in cartesian coordinates due to their long narrow shapes. Compare Fig. 11 in which the vertical axis is the radial coordinates (r) of the baffle plate structure and the horizontal axis is the azimuthal angle coordinates (ϕ). Visible is the stairstep structure of the slit boundaries due to the plates' being modeled in GEANT as sets of 20 concentric layers. In this visualization one can see for each slit boundary, ϕ and r are piecewise linearly related. On the left side the pronounced slope difference of the two pieces produces an angular constriction at smaller r .

Electron tracks were generated uniformly distributed in $p > 2$ GeV/c and θ_p , but with ϕ_p fixed at 12° ; then cuts $x_{Bj} > 0.55$, $W^2 > 4$ GeV², $Q^2 > 6$ GeV² were imposed. These tracks were propagated in the CLEO magnet field, but

More1 baffle upstream/center vertex

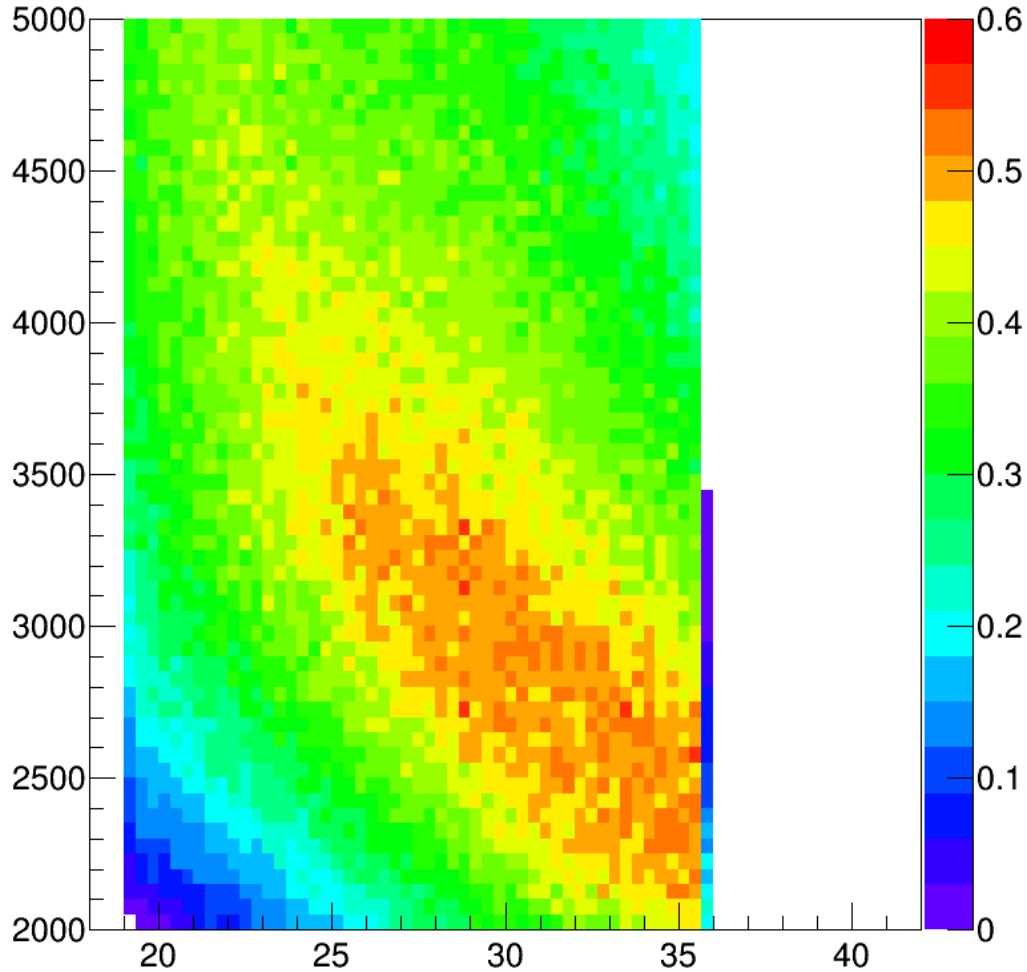


FIG. 5. Acceptance as function of p (MeV/c) vs. θ_p (degrees) for electrons traversing Kryptonite More1 baffles with standard geometry; vertex is halfway between upstream end and center of target.

with no baffles or other materials present. Superposed on the r vs ϕ pictures of the slits in Figs. 12–16 are positions of these tracks; the red points are positions at z corresponding to the front of each baffle plate and the green points are at the z of the back of the plate. We see that for larger values of θ_p (that is, larger r) the shapes of the slits look reasonable to give $\sim 50\%$ acceptance for good events. At small θ_p , the angular constriction cuts into the acceptance.

Figures 17–21 are similar, but for electrons distributed uniformly in ϕ , and in this case Kryptonite More1 baffles were present in the simulation and positions were plotted *only for electrons that got through all 11 baffle plates*.

For upstream electrons, one can see the θ_p acceptance is limited by the outer radius of the first baffle plate. This radius could be increased for a small improvement in acceptance. For the other vertex positions θ_p is limited by the outer radius of the last baffle, which is constrained by the solenoid diameter.

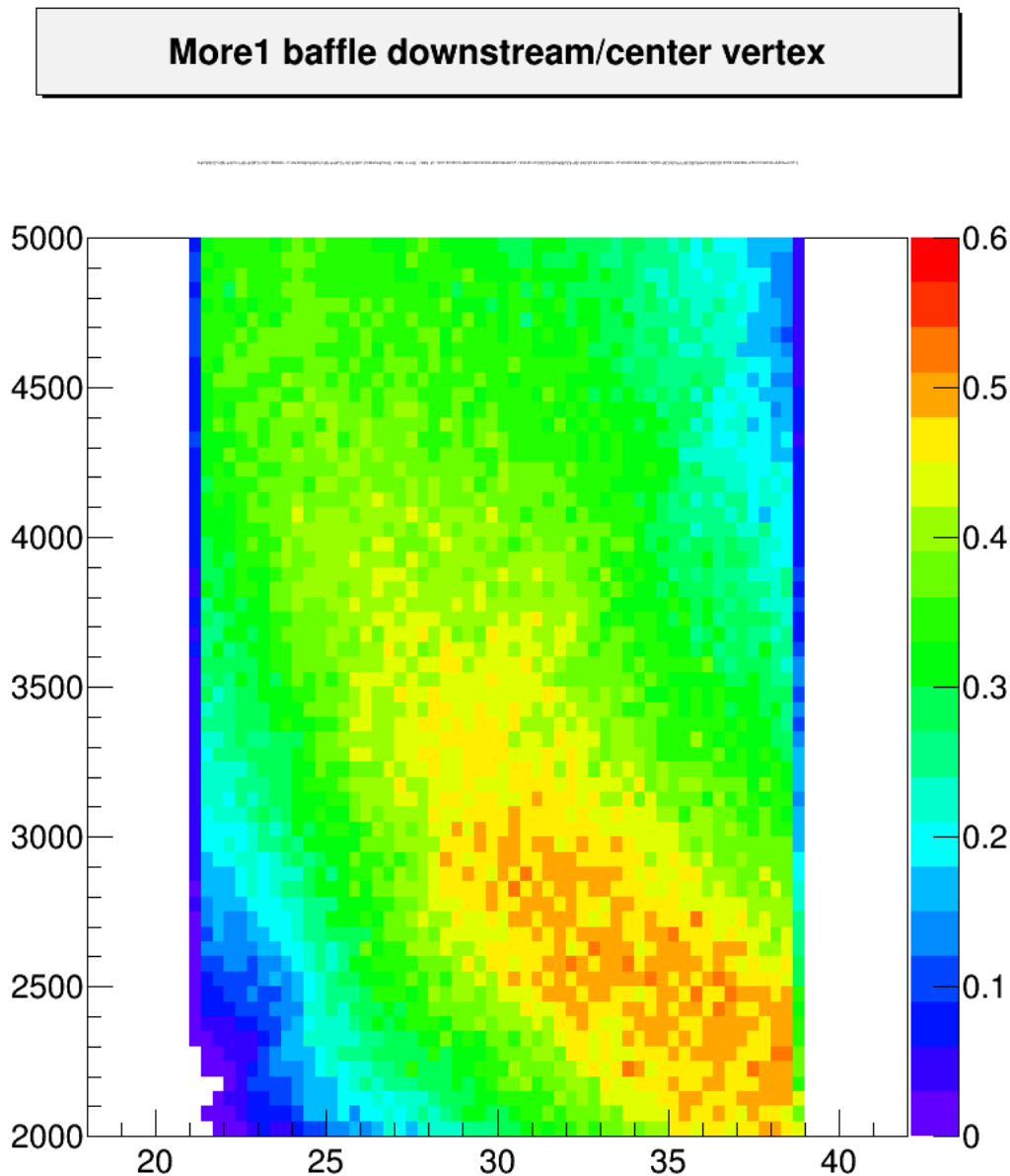


FIG. 6. Acceptance as function of p (MeV/c) vs. θ_p (degrees) for electrons traversing Kryptonite More1 baffles with standard geometry; vertex is halfway between center and downstream end of target.

For all but downstream electrons, the ϕ acceptance is defined by the right edge of the slit in the first baffle and the left edges of the slit in the last baffle and, to some extent, the first two baffles. Elsewhere one sees gaps, where electrons that would be accepted by one slit are blocked by another; note especially the right edge of the last baffles.

The situation is different for electrons from the downstream end. These enter the slit in the first plate from the “bottom” (minimum r). As a result the ϕ acceptance for these electrons (again, in the absence of the inner ring) is determined by the severely constrained angular width of the first plate’s slits at the innermost radius.

Figure 22 is the same but with electrons from all five vertex positions superposed. Gaps where no electrons that clear the baffles go are evident. Increasingly large gaps along the right edge in the later plates probably are due to the fact that the integrated field for the CLEO solenoid is slightly lower than that for the BaBar solenoid for which the baffles originally were designed. Adjustments to the long edges of the slits would give a better match to the CLEO

More1 baffle downstream vertex

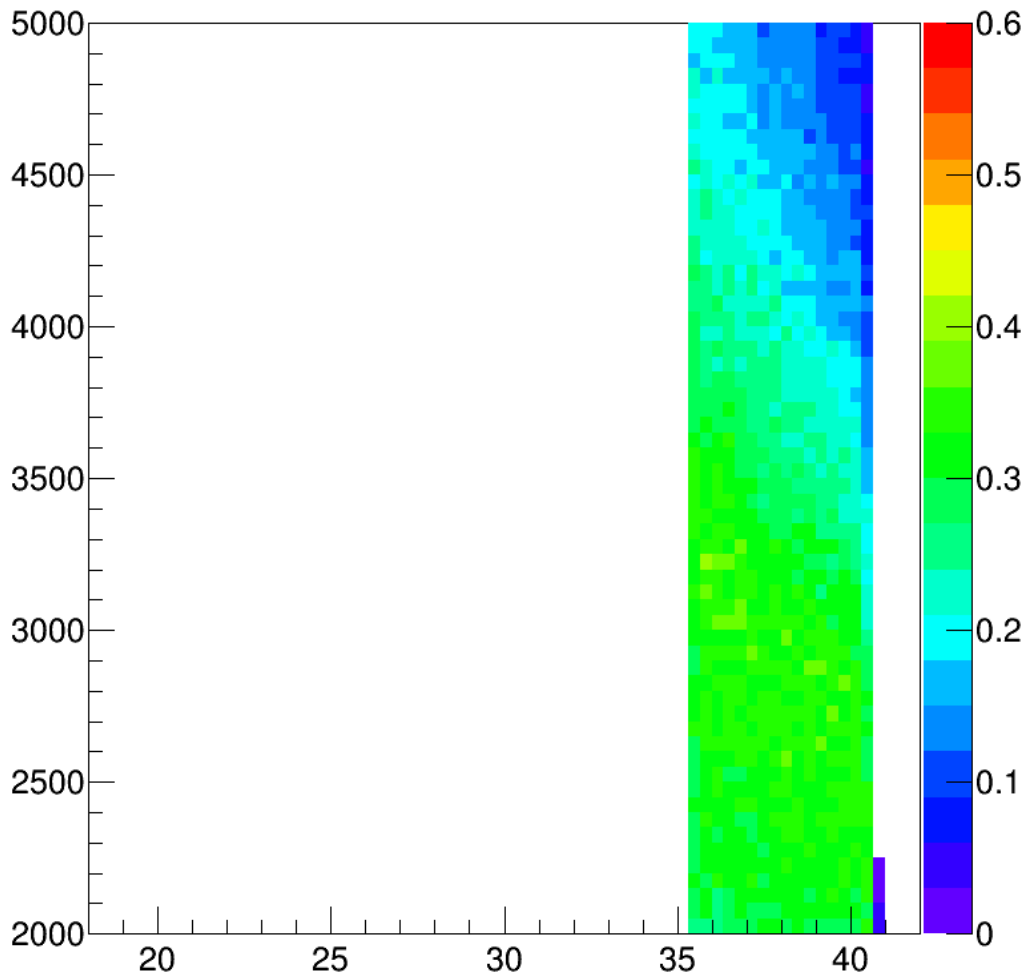


FIG. 7. Acceptance as function of p (MeV/c) vs. θ_p (degrees) for electrons traversing Kryptonite More1 baffles with standard geometry; vertex is at downstream end of target.

field.

Figure 23 is similar, but for photons rather than electrons. The defining edges for the photons that clear the baffles are the right edge of the first plate and the left edge of the last plate. The resulting photon hot spot at small radius (within detector acceptance) and near the left edge of the slit has been seen in previous work. Blocking these photons at or after the last baffle plate would reduce straight throughs; the small θ_p constrictions in the upstream baffles do not. Note also that the photon acceptance will be highly sensitive to small changes in the position of the right slit edge in the first baffle.

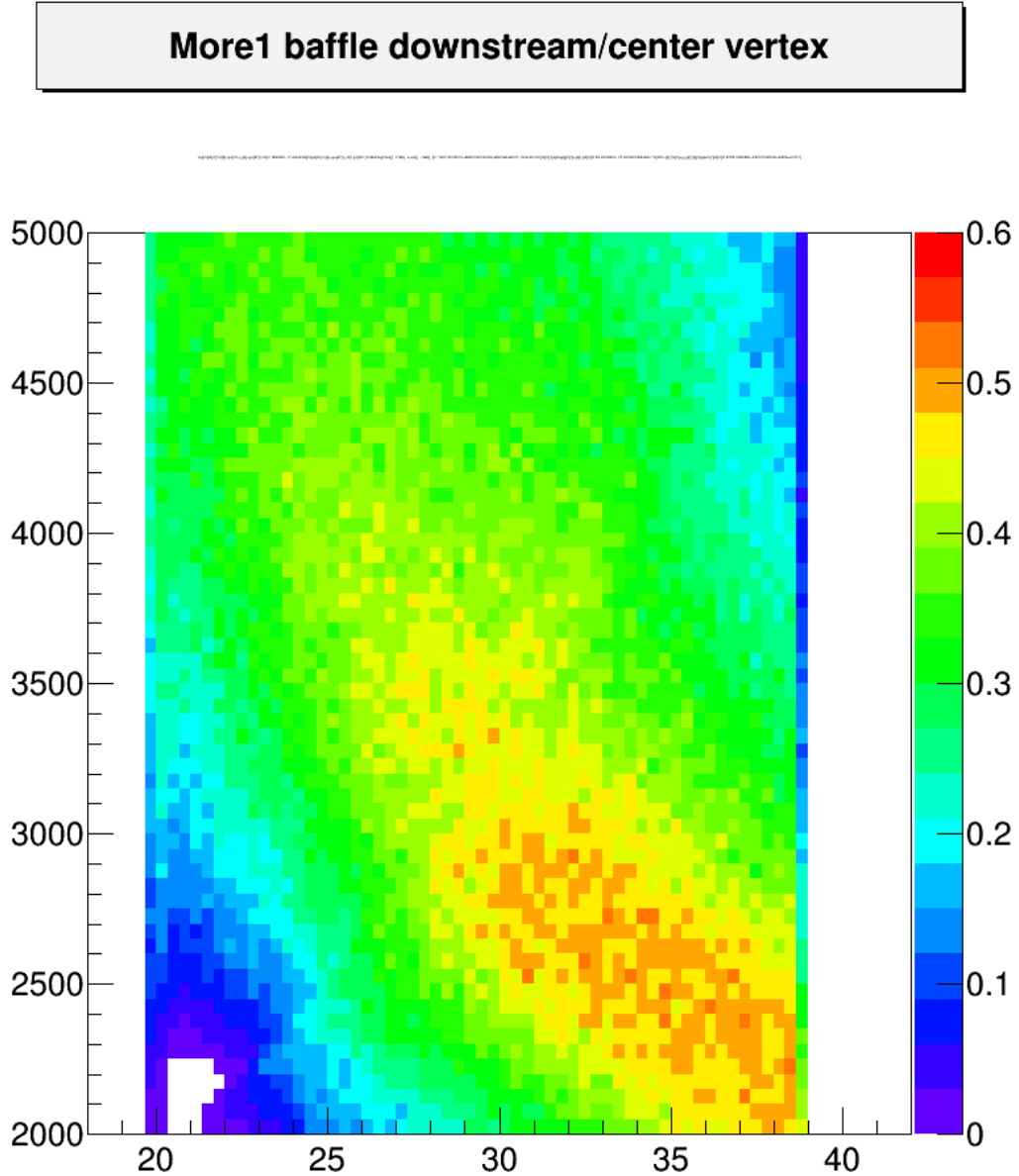


FIG. 8. Acceptance as function of p (MeV/c) vs. θ_p (degrees) for electrons traversing Kryptonite More1 baffles with inner rings removed; vertex is halfway between center and downstream end of target.

V. 6.6 GEV/C BEAM

Here I consider performance of the More1 baffles for 6.6 GeV/c beam. I look at the kinematics of the rightmost points in the lower (green dots) series of Figure 2.6 of the PVDIS proposal [2]. I still require $p > 2$ GeV/c and $W^2 > 4$ GeV², but the other cuts are $Q^2 > 3.5$ GeV/c² and $x_{bj} > 0.45$ rather than the requirements $Q^2 > 6$ GeV/c², and $x_{bj} > 0.55$ used for 11 GeV/c.

A plot of energy versus scattering angle for inelastic electrons traversing Kryptonite More1 baffles with inner ring removed and with these cuts is shown in Fig. 24 (magenta points) along with black dots representing 11 GeV electrons with their kinematic cuts, both superimposed on a color plot of acceptance similar to Fig. 3. This shows the acceptance for the 6.6 GeV tracks is down compared to the 11 GeV data by roughly 20%.

More1 baffle downstream vertex

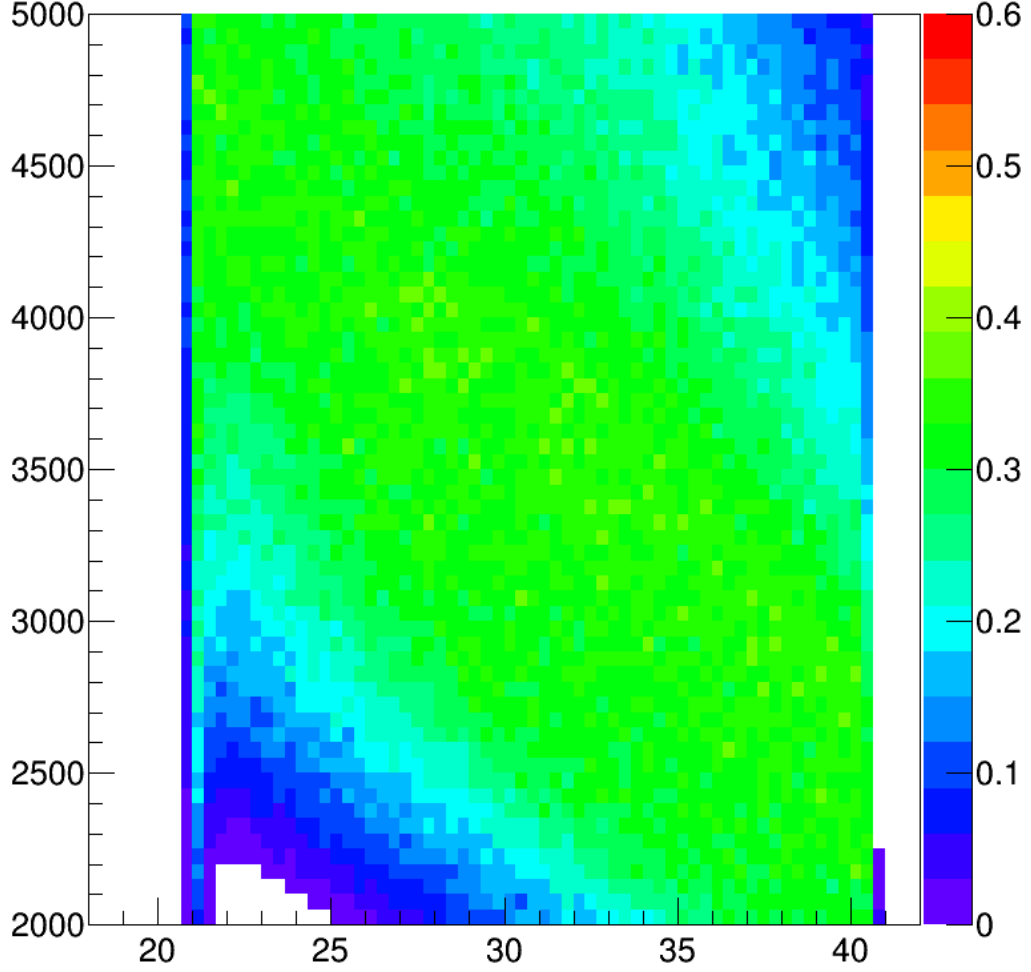


FIG. 9. Acceptance as function of p (MeV/c) vs. θ_p (degrees) for electrons traversing Kryptonite More1 baffles with inner rings removed; vertex is at downstream end of target.

Figures 25 to 34 are analogous to figures 12 to 21, but for 6.6 GeV beam. Figures 25 to 29 are for electron tracks generated uniformly distributed in $p > 2$ GeV/c and θ_p , but with ϕ_p fixed at 12° ; then the cuts discussed above were imposed. These tracks were propagated in the CLEO magnet field, but with no baffles or other materials present. The red points are positions at z corresponding to the front of each baffle plate and the green points are at the z of the back of the plate. For 11 GeV the stripes thereby generated widen through dispersion but are roughly centered in the slits in each plate, but we see for the lower momentum 6.6 GeV data the stripes turn faster in the field and start to run up against the slit edges in the last baffles. Clearly acceptance will be lost for lower momentum tracks with ϕ_p above about 12° relative to each segment.

Figures 30 to 34 are similar, but for electrons distributed uniformly in ϕ , and in this case Kryptonite More1 baffles (with the inner ring removed) were present in the simulation and positions were plotted *only for electrons that got*

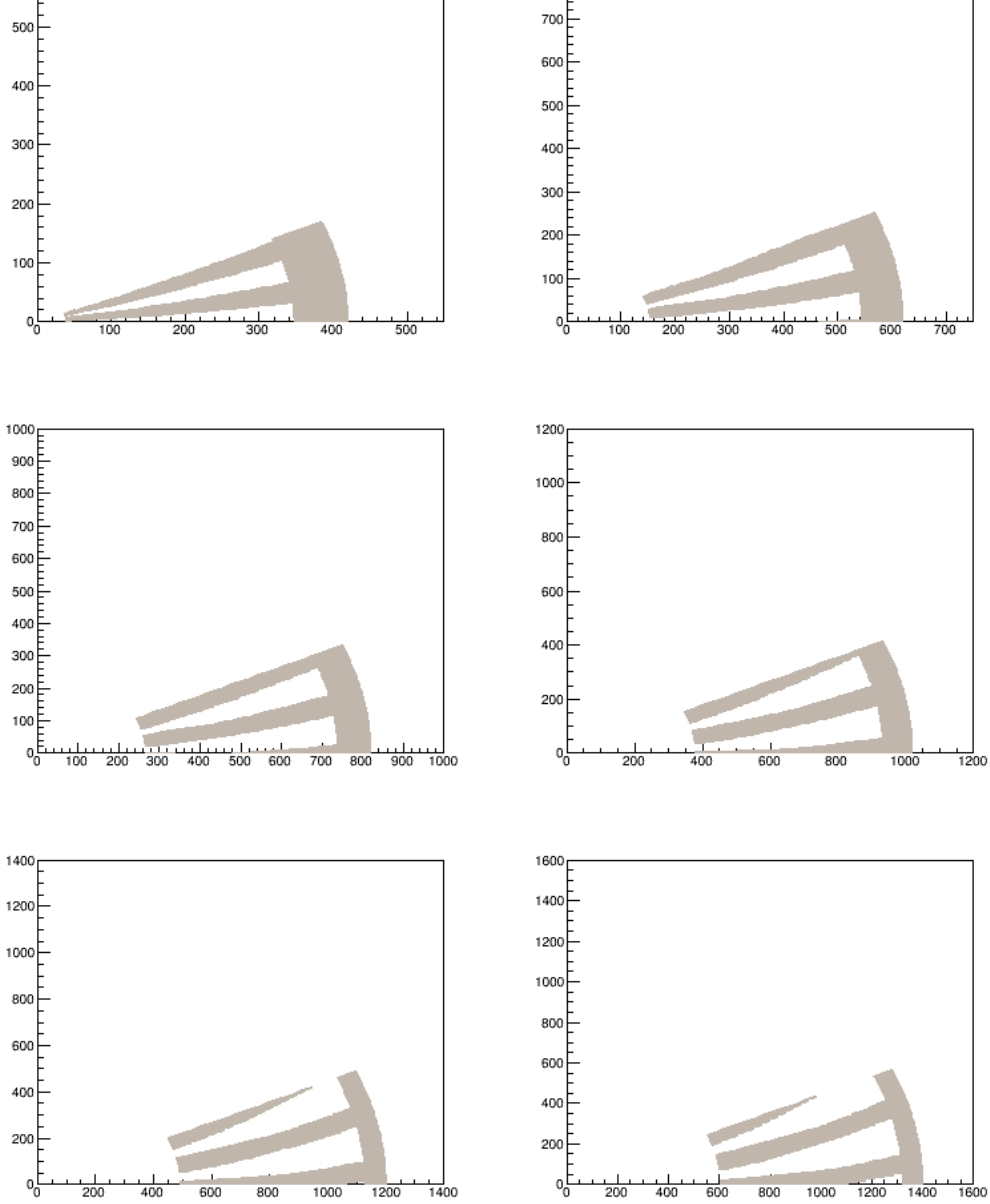


FIG. 10. 24° wide segments of the odd numbered baffle plates drawn in cartesian coordinates (in mm). Inner rings are omitted.

through all 11 baffle plates. The limiting apertures generally are the same as was the case for 11 GeV. For upstream electrons, one can see the θ_p acceptance is limited by the outer radius of the first baffle plate. For mid target electrons θ_p is limited by the last baffle plate, and for downstream electrons θ_p is limited by kinematics.

For all but downstream electrons, the ϕ acceptance is defined by the right edge of the slit in the first baffle and the left edge of the slit in the last baffle. For electrons from the downstream end the ϕ acceptance (in the absence of the inner ring) is determined by the severely constrained angular width of the first plate's slits at the innermost radius.

VI. BAFFLE OPTIMIZATION

A few changes to the baffle shapes would give a better match to the trajectories in the CLEO field.

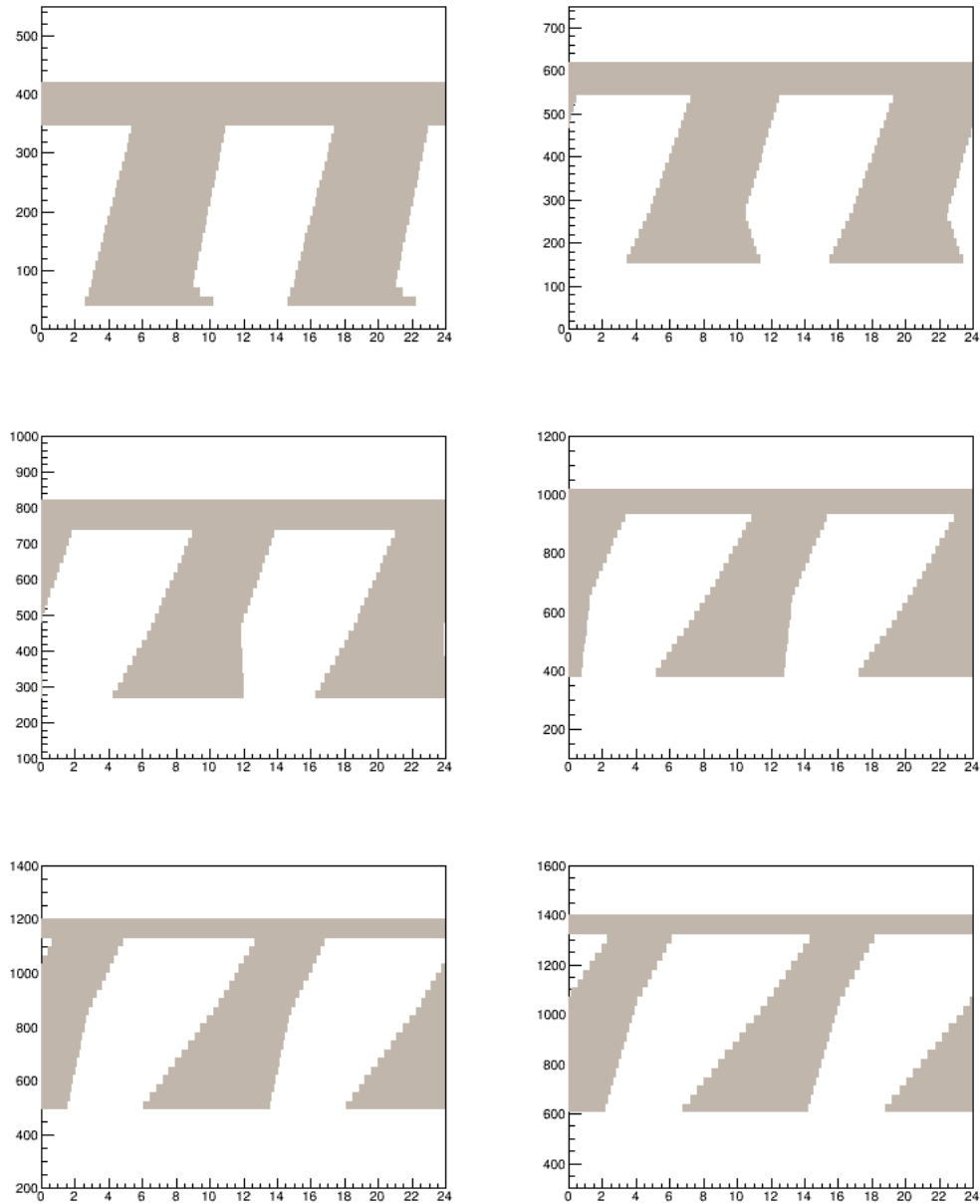


FIG. 11. 24° wide segments of the odd numbered baffle plates; the vertical axis is the radial coordinates (r , in mm) of the baffle plate structure and the horizontal axis is the azimuthal angle coordinates (ϕ , in degrees). Inner rings are omitted.

- The inner rings on at least the first few upstream plates should be eliminated, if mechanically possible, to recover acceptance from the downstream end of the target.
- The outer radius of the first few plates should be increased to improve acceptance from the upstream end of the target.
- The angular constrictions at small radius in the upstream baffles should be relaxed.
- Slight adjustments to the long edges of the slits, especially the right edges of the downstream slits, should be made to reduce gaps.

Such a modified baffle set is shown in Fig. 35. The left and outer edges of the last plate's slits and the right edge

Upstream vertex

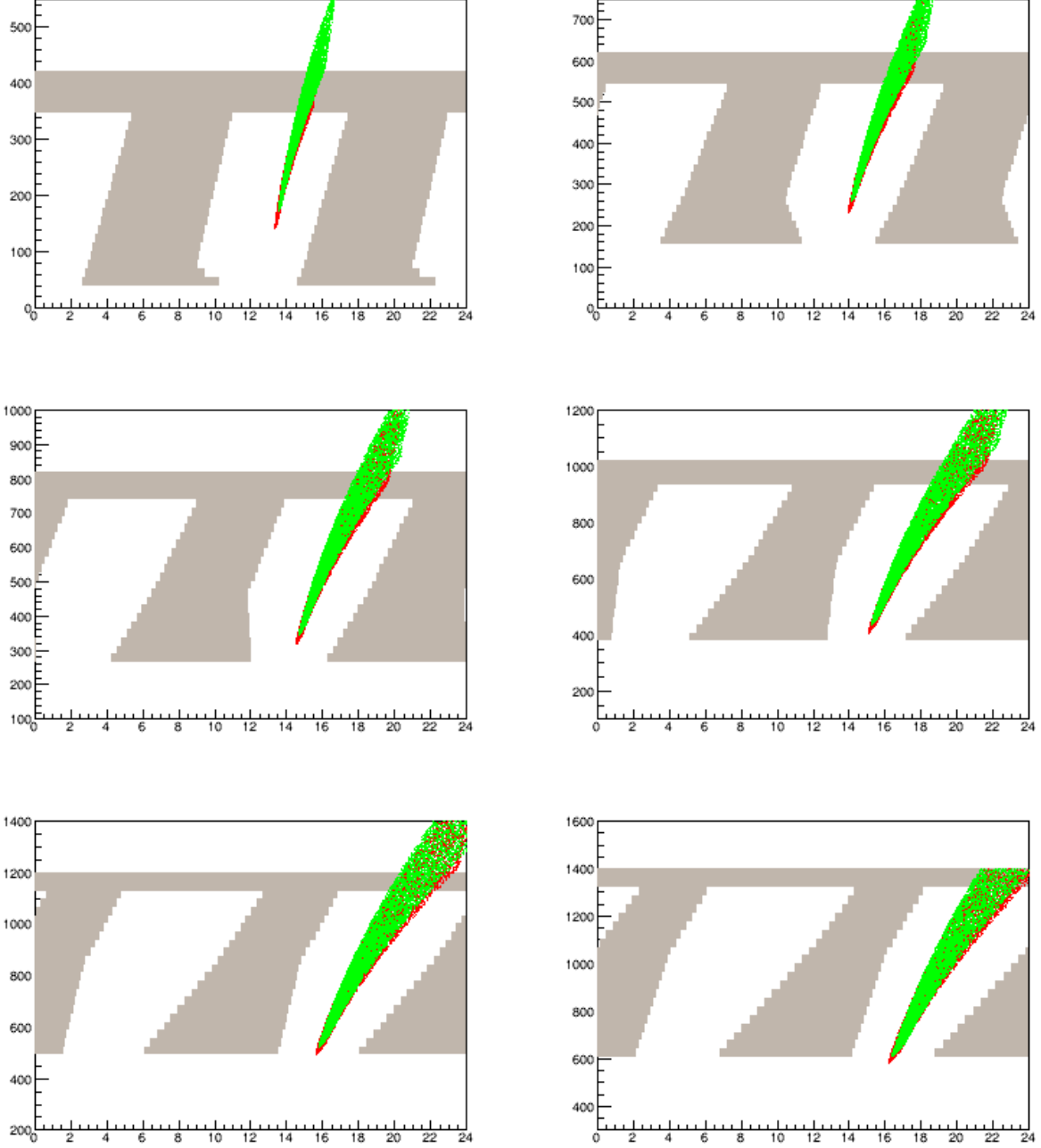


FIG. 12. Positions of electron tracks with $p > 2 \text{ GeV}/c$, $\phi_p = 12^\circ$, $x_{Bj} > 0.55$, $W^2 > 4 \text{ GeV}^2$, $Q^2 > 6 \text{ GeV}^2$, and vertex at the upstream end of the target for each of the odd numbered baffle plates. Red (green) points are at z corresponding to the upstream (downstream) face of each plate. Baffles were not present in the simulation but their shapes are drawn for reference.

Mid/upstream vertex

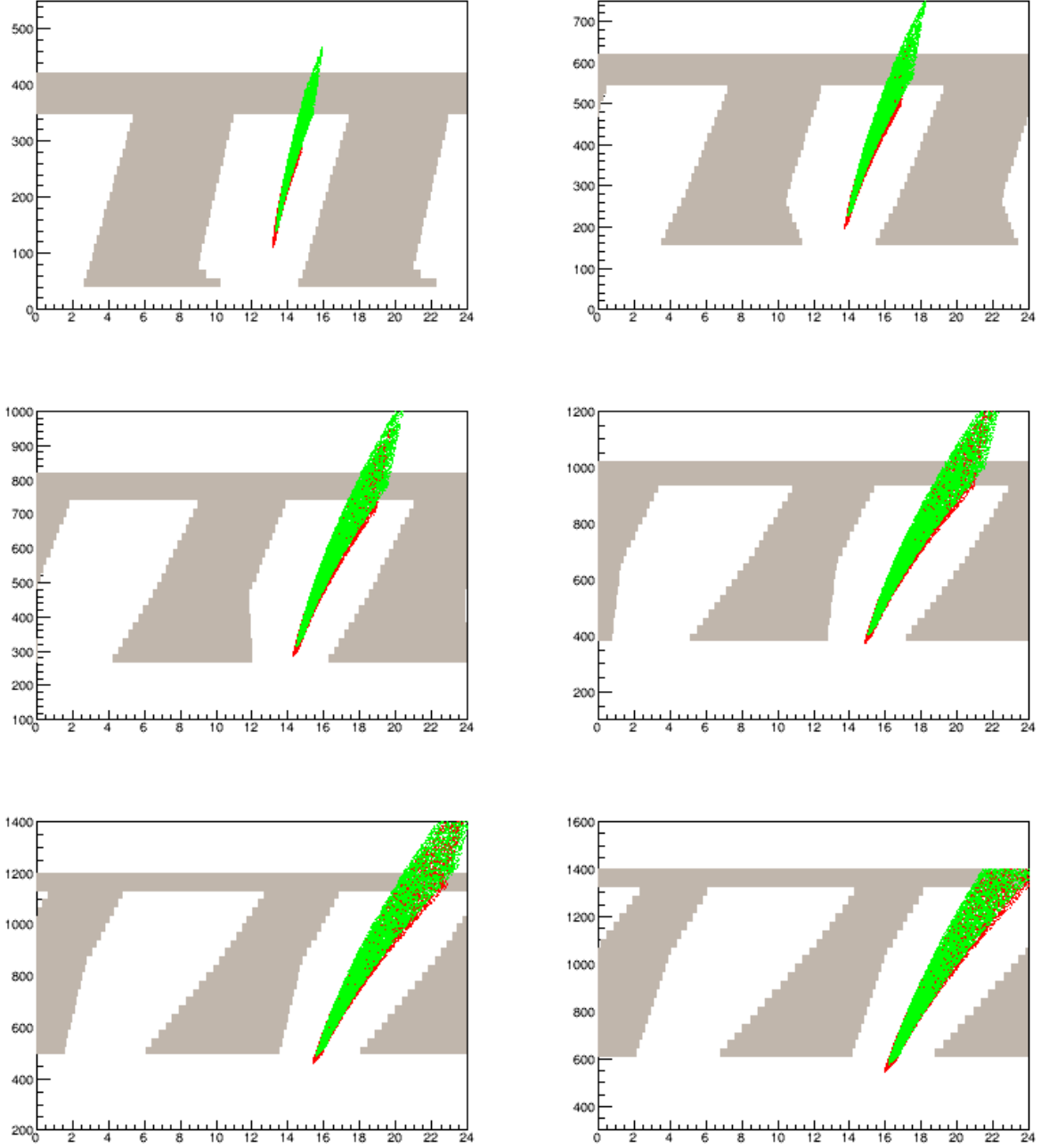


FIG. 13. Positions of electron tracks with $p > 2$ GeV/c, $\phi_p = 12^\circ$, $x_{Bj} > 0.55$, $W^2 > 4$ GeV², $Q^2 > 6$ GeV², and vertex halfway the upstream end and center of the target for each of the odd numbered baffle plates. Red (green) points are at z corresponding to the upstream (downstream) face of each plate. Baffles were not present in the simulation but their shapes are drawn for reference.

Middle vertex

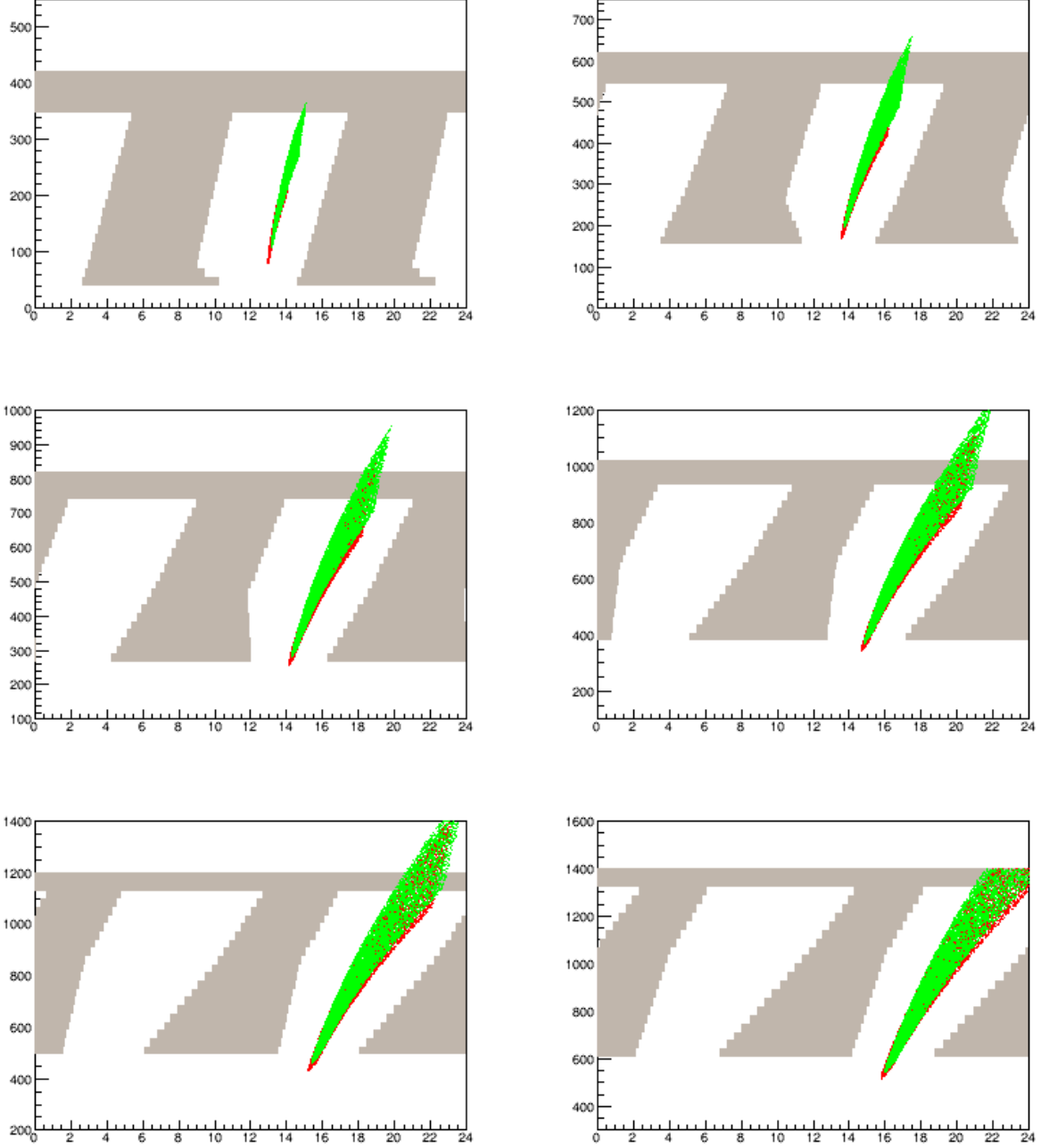


FIG. 14. Positions of electron tracks with $p > 2 \text{ GeV}/c$, $\phi_p = 12^\circ$, $x_{Bj} > 0.55$, $W^2 > 4 \text{ GeV}^2$, $Q^2 > 6 \text{ GeV}^2$, and vertex at the center of the target for each of the odd numbered baffle plates. Red (green) points are at z corresponding to the upstream (downstream) face of each plate. Baffles were not present in the simulation but their shapes are drawn for reference.

Mid/downstream vertex

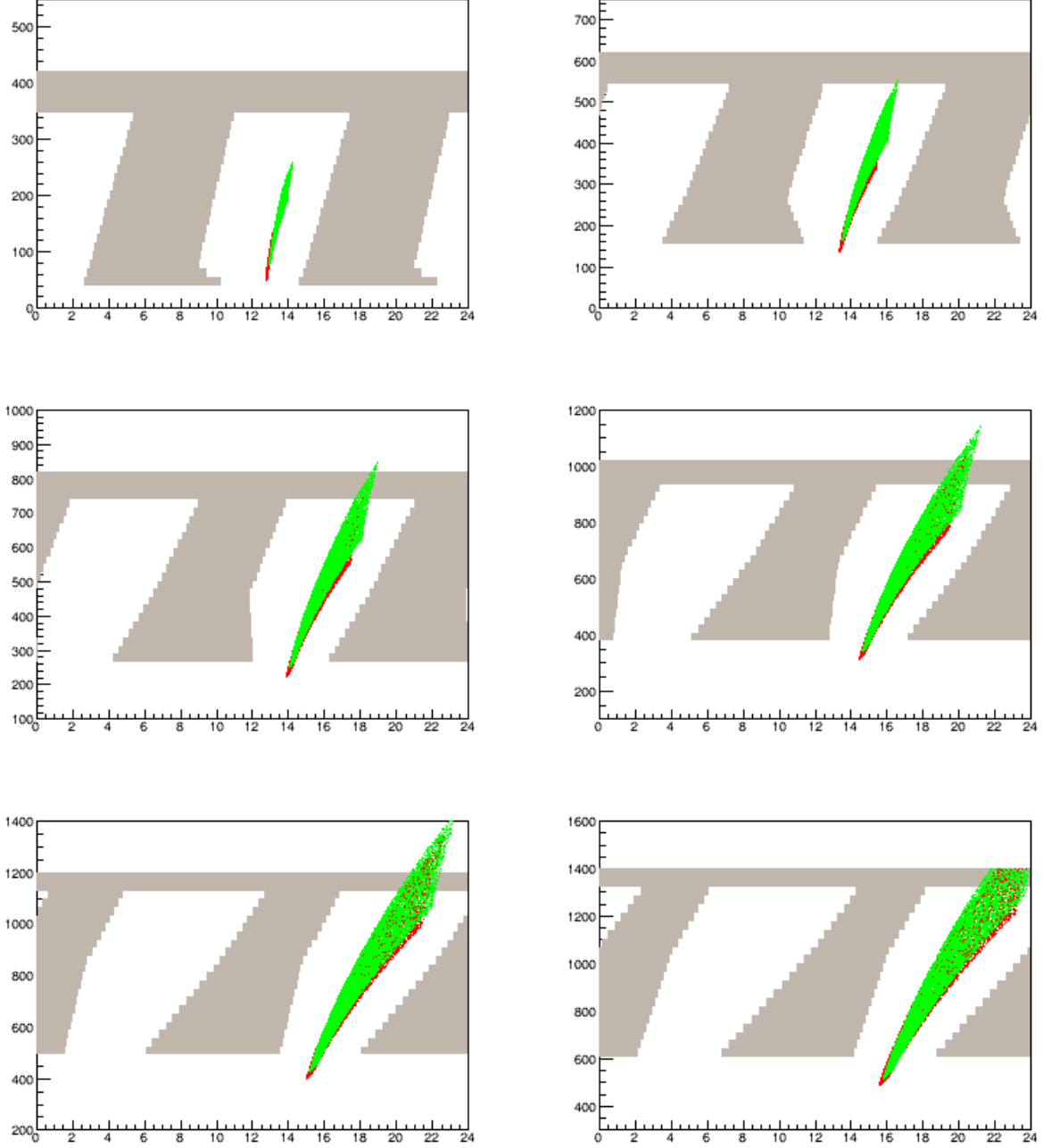


FIG. 15. Positions of electron tracks with $p > 2$ GeV/c, $\phi_p = 12^\circ$, $x_{Bj} > 0.55$, $W^2 > 4$ GeV², $Q^2 > 6$ GeV², and vertex halfway between the center and downstream end of the target for each of the odd numbered baffle plates. Red (green) points are at z corresponding to the upstream (downstream) face of each plate. Baffles were not present in the simulation but their shapes are drawn for reference.

Downstream vertex

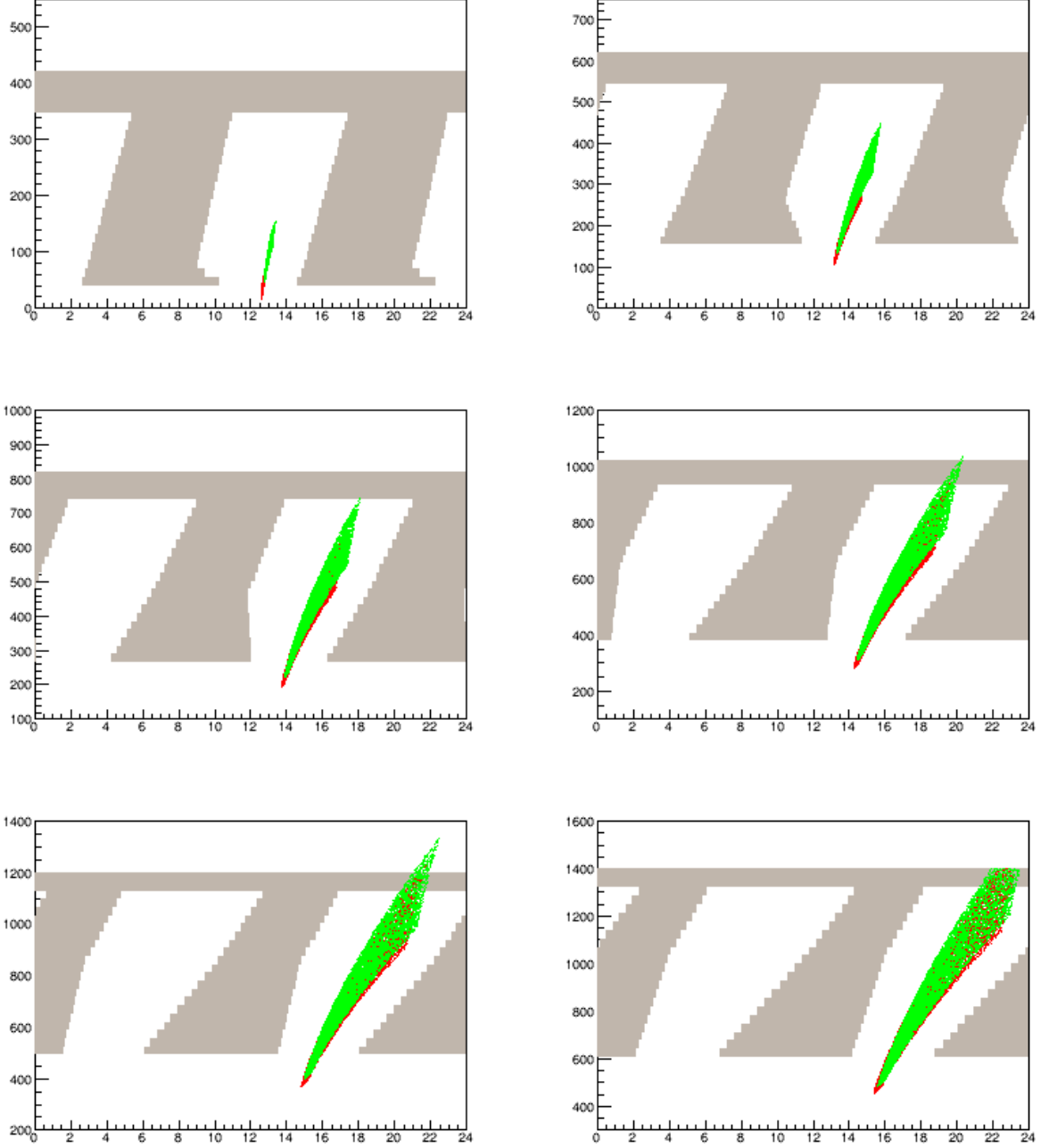


FIG. 16. Positions of electron tracks with $p > 2 \text{ GeV}/c$, $\phi_p = 12^\circ$, $x_{Bj} > 0.55$, $W^2 > 4 \text{ GeV}^2$, $Q^2 > 6 \text{ GeV}^2$, and vertex at the downstream end of the target for each of the odd numbered baffle plates. Red (green) points are at z corresponding to the upstream (downstream) face of each plate. Baffles were not present in the simulation but their shapes are drawn for reference.

Upstream vertex

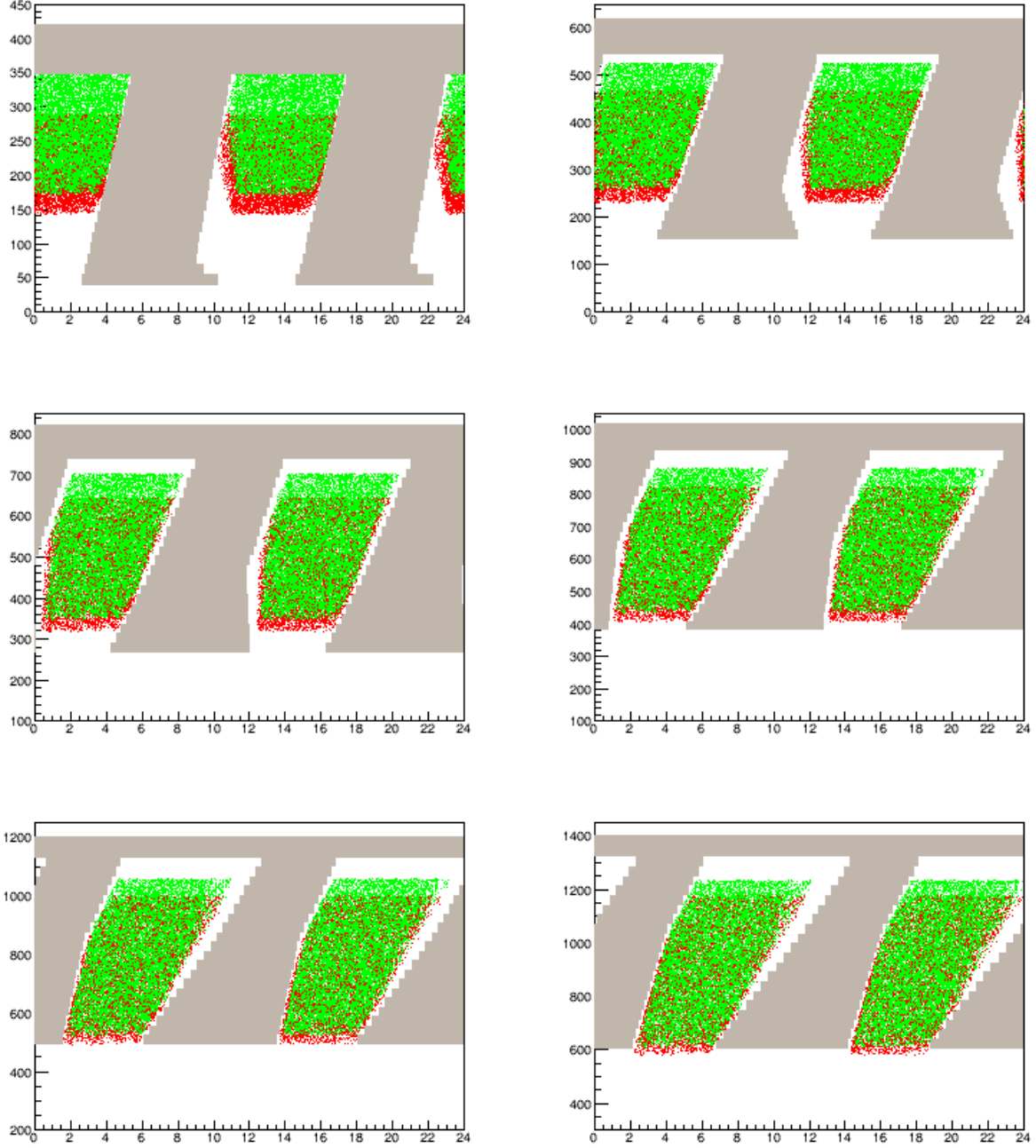


FIG. 17. Positions of electron tracks with $p > 2 \text{ GeV}/c$, $x_{Bj} > 0.55$, $W^2 > 4 \text{ GeV}^2$, $Q^2 > 6 \text{ GeV}^2$, and vertex at the upstream end of the target for each of the odd numbered baffle plates. Kryptonite More1 baffles (inner ring removed) were present in the simulation, and only electrons which passed through all 11 baffle plates are shown. Red (green) points are at z corresponding to the upstream (downstream) face of each plate.

Mid/upstream vertex

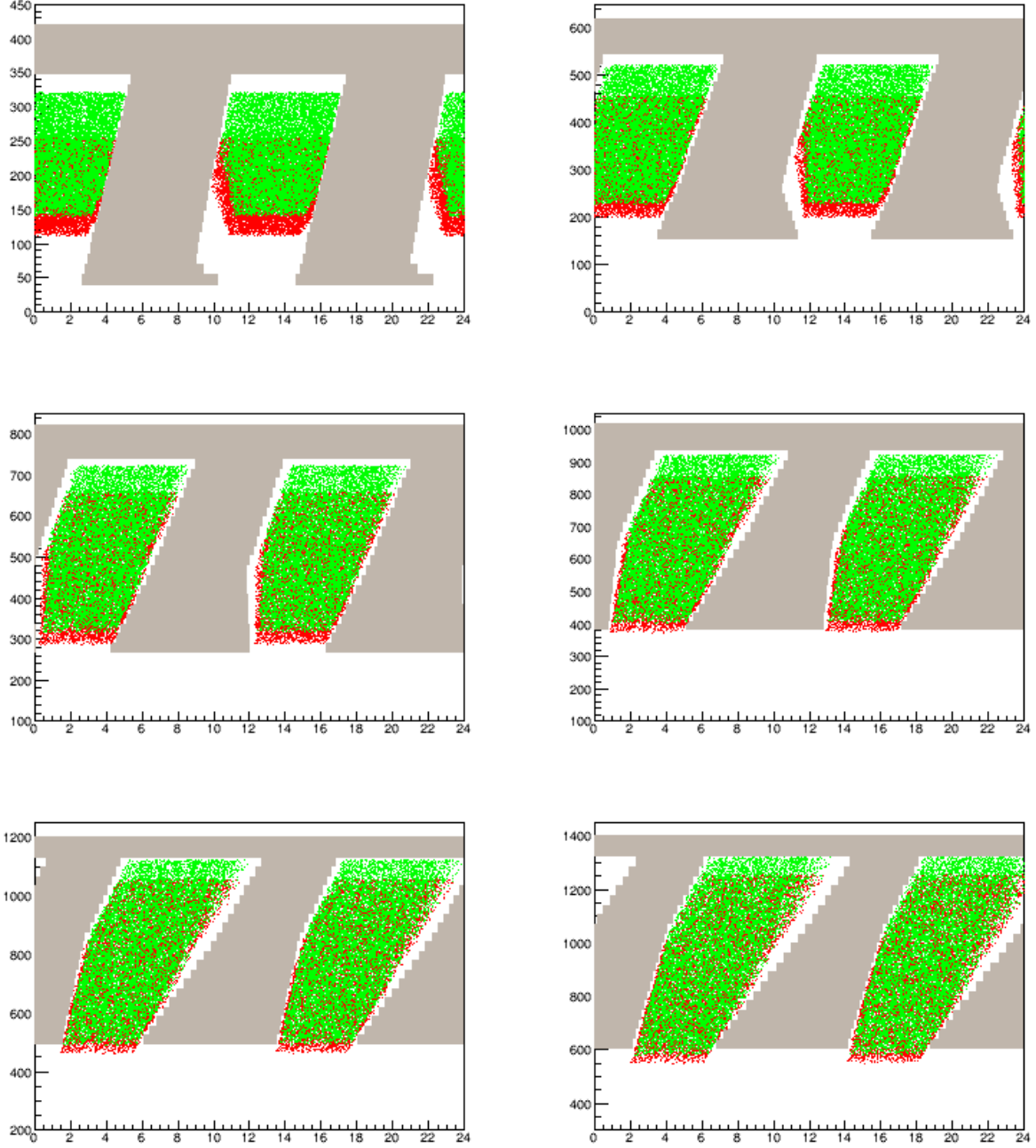


FIG. 18. Positions of electron tracks with $p > 2 \text{ GeV}/c$, $x_{Bj} > 0.55$, $W^2 > 4 \text{ GeV}^2$, $Q^2 > 6 \text{ GeV}^2$, and vertex halfway the upstream end and center of the target for each of the odd numbered baffle plates. Kryptonite More1 baffles (inner ring removed) were present in the simulation, and only electrons which passed through all 11 baffle plates are shown. Red (green) points are at z corresponding to the upstream (downstream) face of each plate.

Middle vertex

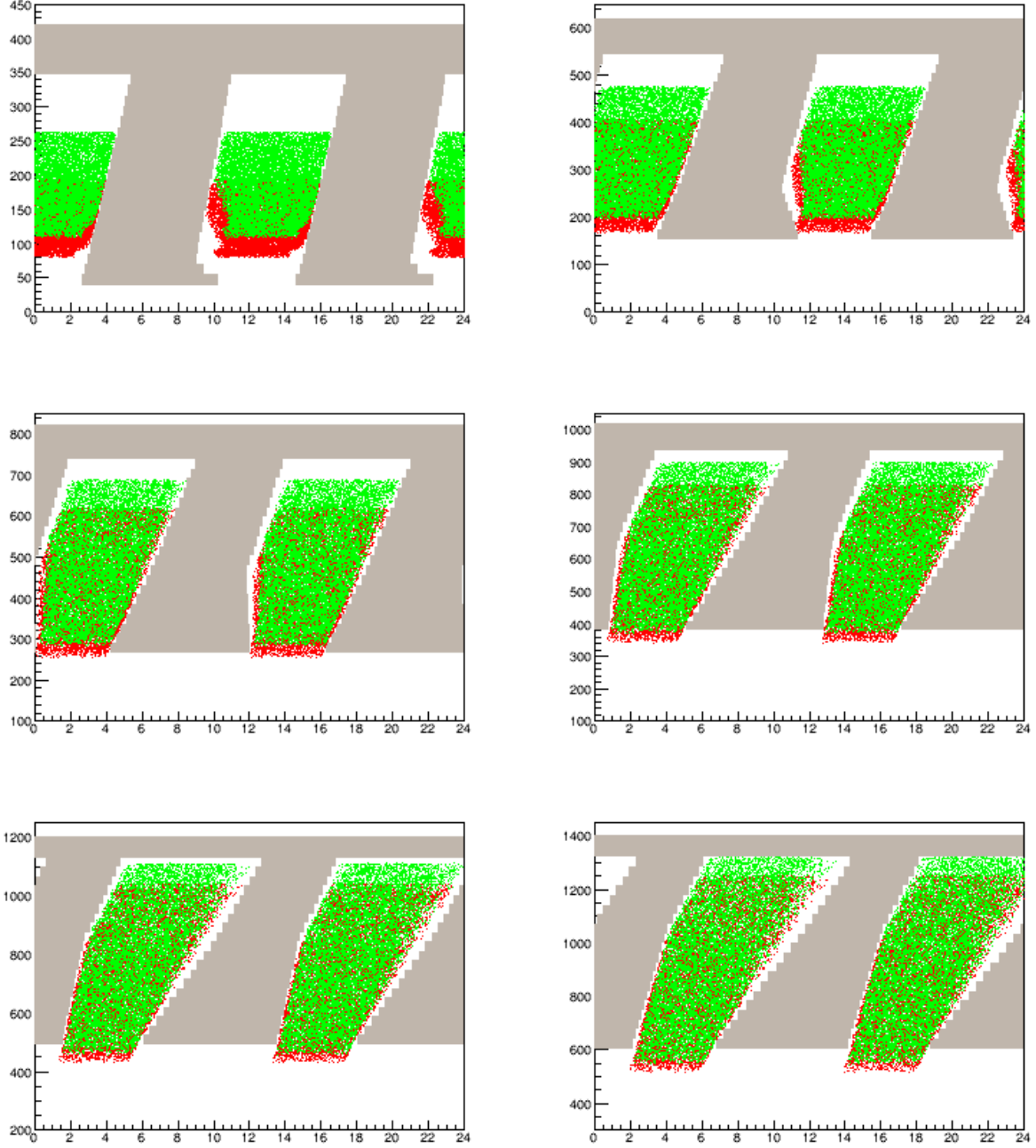


FIG. 19. Positions of electron tracks with $p > 2 \text{ GeV}/c$, $x_{Bj} > 0.55$, $W^2 > 4 \text{ GeV}^2$, $Q^2 > 6 \text{ GeV}^2$, and vertex at the center of the target for each of the odd numbered baffle plates. Kryptonite More1 baffles (inner ring removed) were present in the simulation, and only electrons which passed through all 11 baffle plates are shown. Red (green) points are at z corresponding to the upstream (downstream) face of each plate.

Mid/downstream vertex

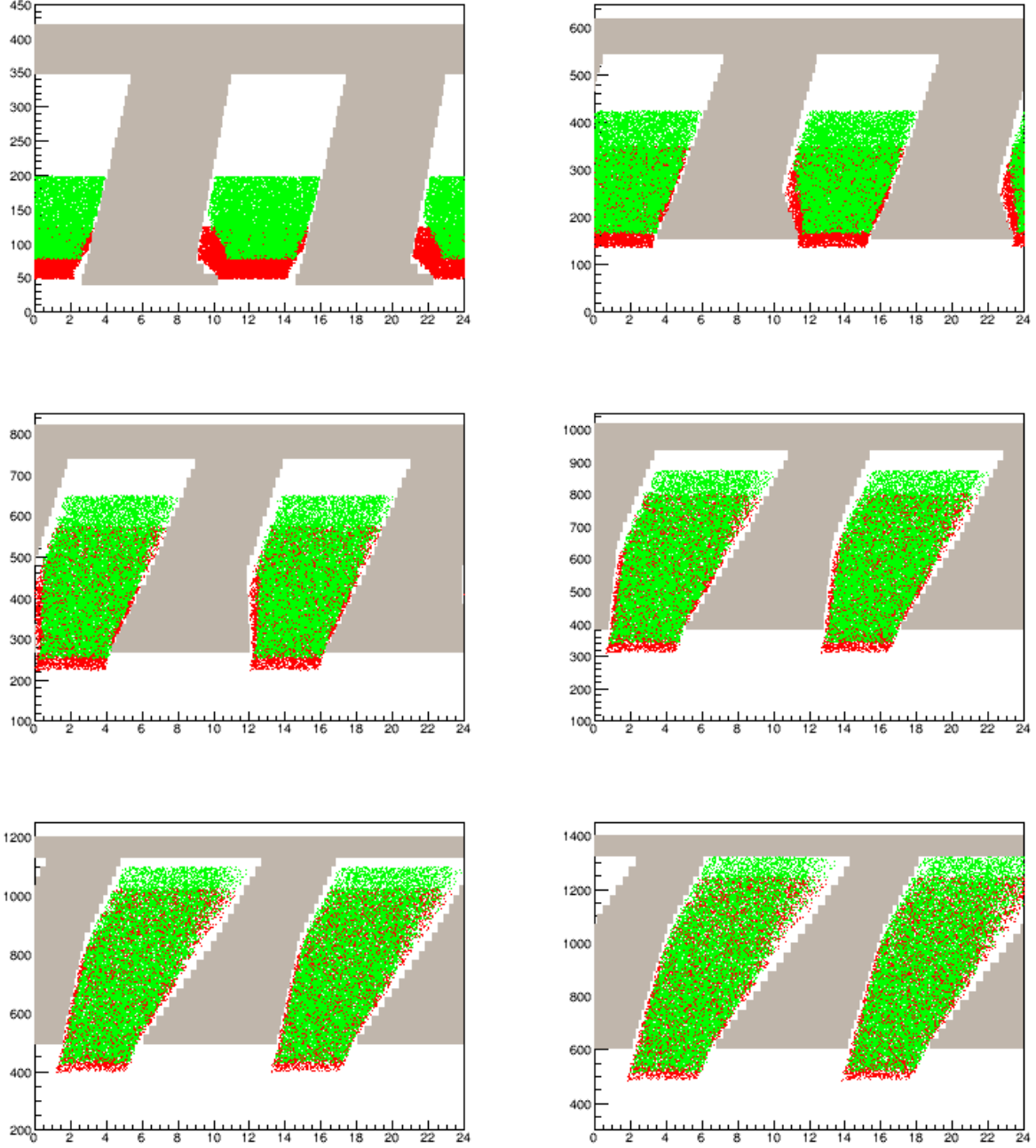


FIG. 20. Positions of electron tracks with $p > 2 \text{ GeV}/c$, $x_{Bj} > 0.55$, $W^2 > 4 \text{ GeV}^2$, $Q^2 > 6 \text{ GeV}^2$, and vertex halfway between the center and downstream end of the target for each of the odd numbered baffle plates. Kryptonite More1 baffles (inner ring removed) were present in the simulation, and only electrons which passed through all 11 baffle plates are shown. Red (green) points are at z corresponding to the upstream (downstream) face of each plate.

Downstream vertex

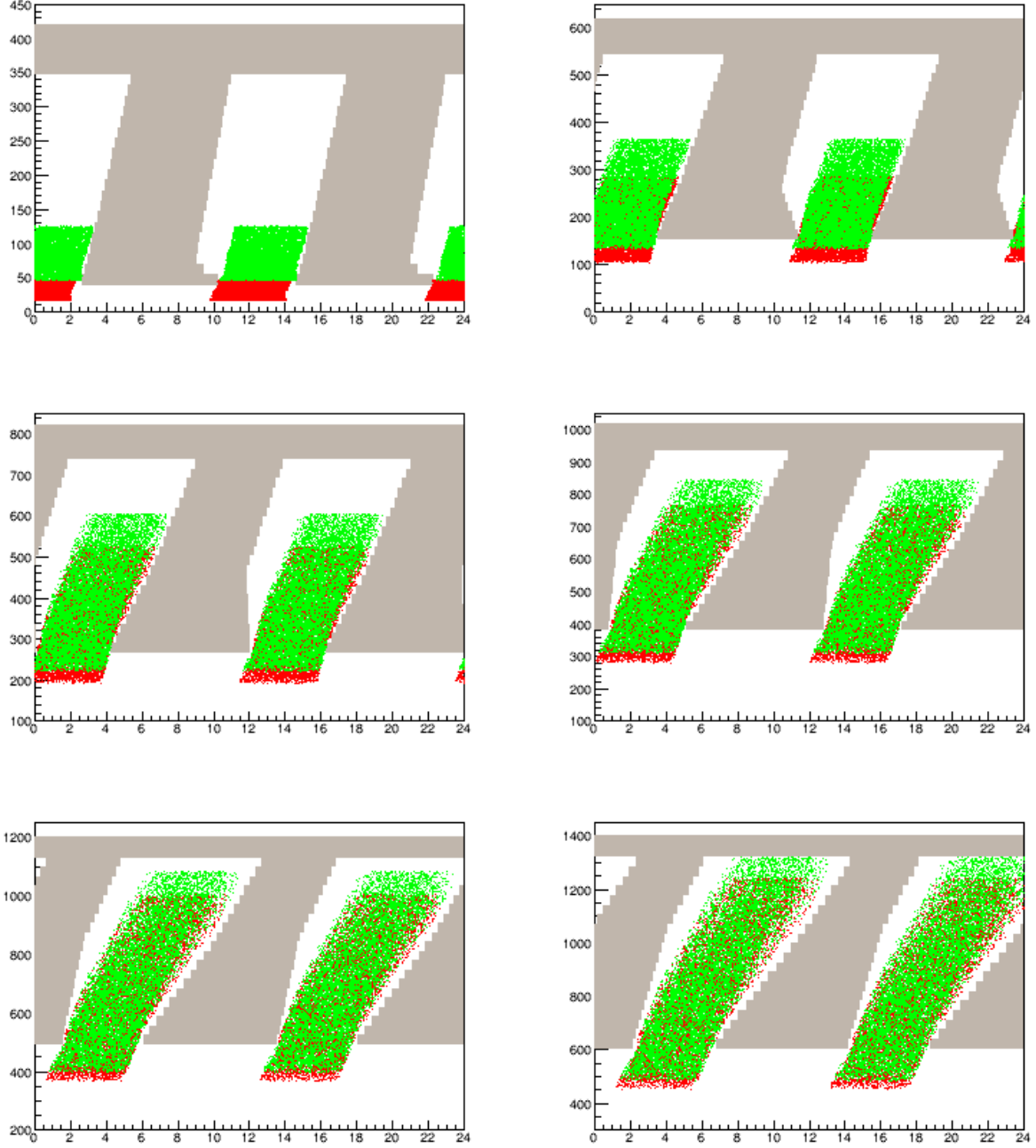


FIG. 21. Positions of electron tracks with $p > 2 \text{ GeV}/c$, $x_{Bj} > 0.55$, $W^2 > 4 \text{ GeV}^2$, $Q^2 > 6 \text{ GeV}^2$, and vertex at the downstream end of the target for each of the odd numbered baffle plates. Kryptonite More1 baffles (inner ring removed) were present in the simulation, and only electrons which passed through all 11 baffle plates are shown. Red (green) points are at z corresponding to the upstream (downstream) face of each plate.

5 vertex

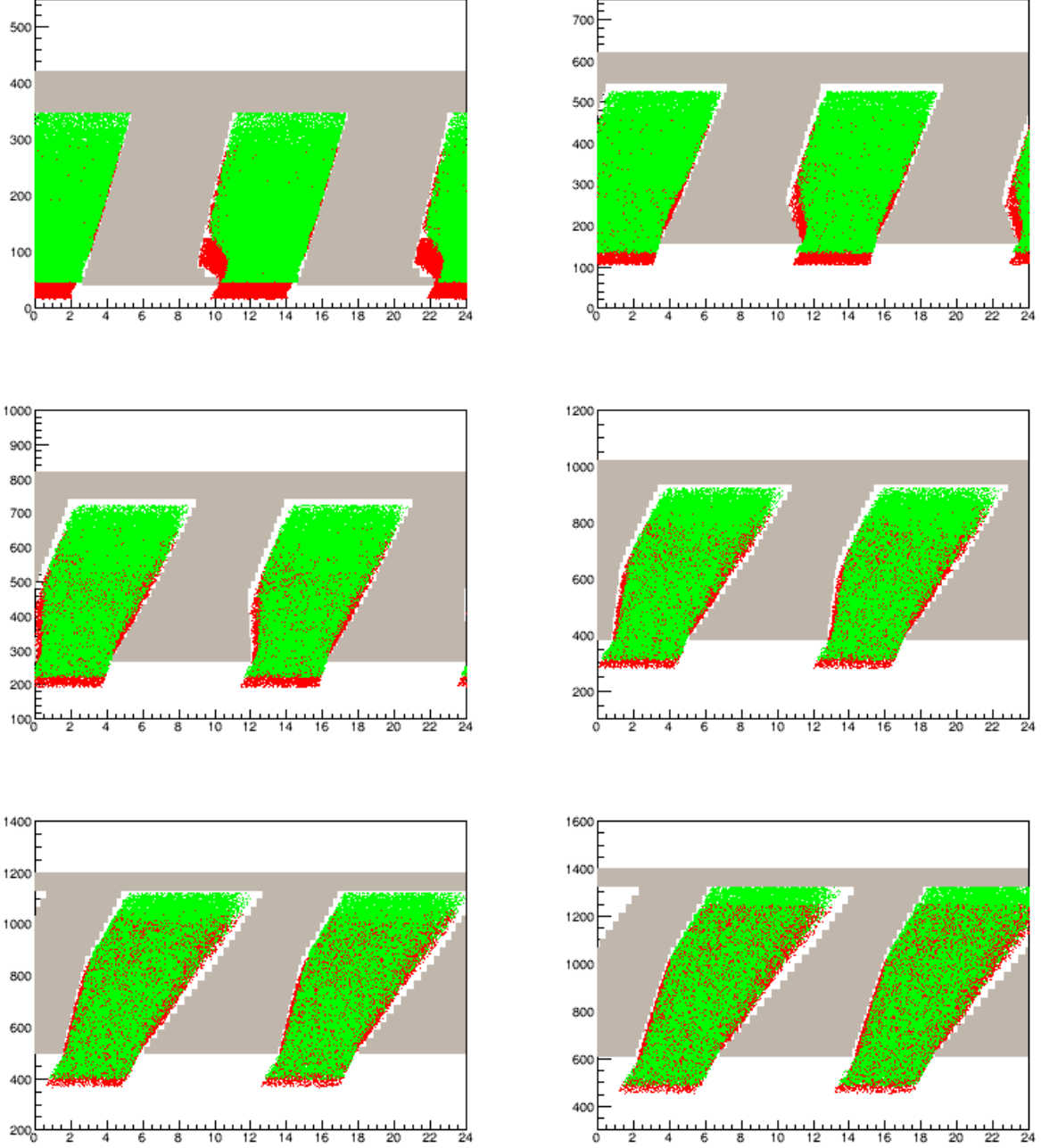


FIG. 22. Positions of electron tracks with $p > 2 \text{ GeV}/c$, $x_{Bj} > 0.55$, $W^2 > 4 \text{ GeV}^2$, $Q^2 > 6 \text{ GeV}^2$, and vertex at any of five positions in the target (upstream end, center, downstream end, or halfway between). Kryptonite More1 baffles (inner ring removed) were present in the simulation, and only electrons which passed through all 11 baffle plates are shown. Red (green) points are at z corresponding to the upstream (downstream) face of each plate.

Neutrals

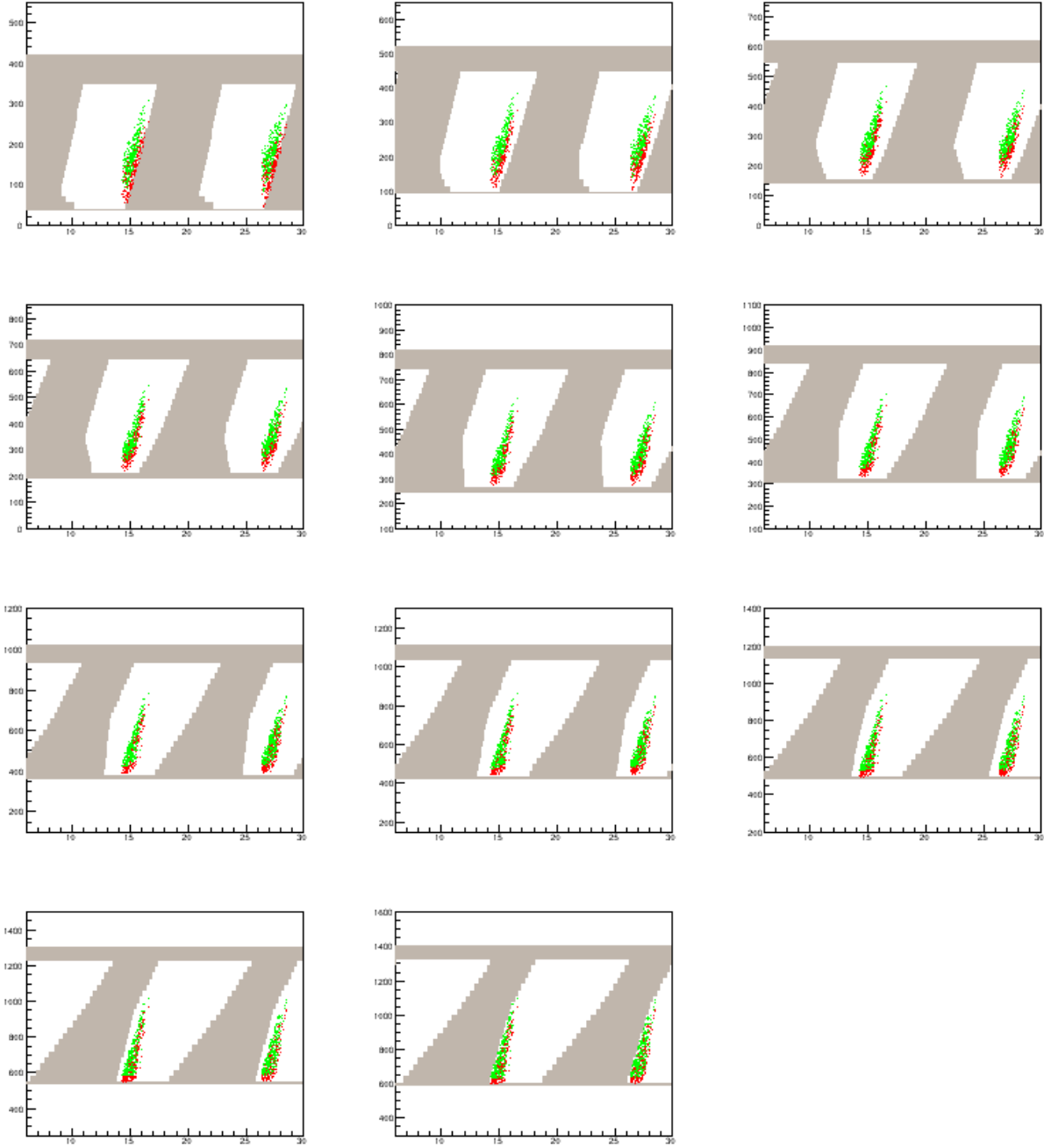


FIG. 23. Positions of photon tracks with vertex at any position in the target (upstream end, center, downstream end, or halfway between). Kryptonite More1 baffles were present in the simulation, and only photons which passed through all 11 baffle plates are shown. Red (green) points are at z corresponding to the upstream (downstream) face of each plate.

More1 baffle

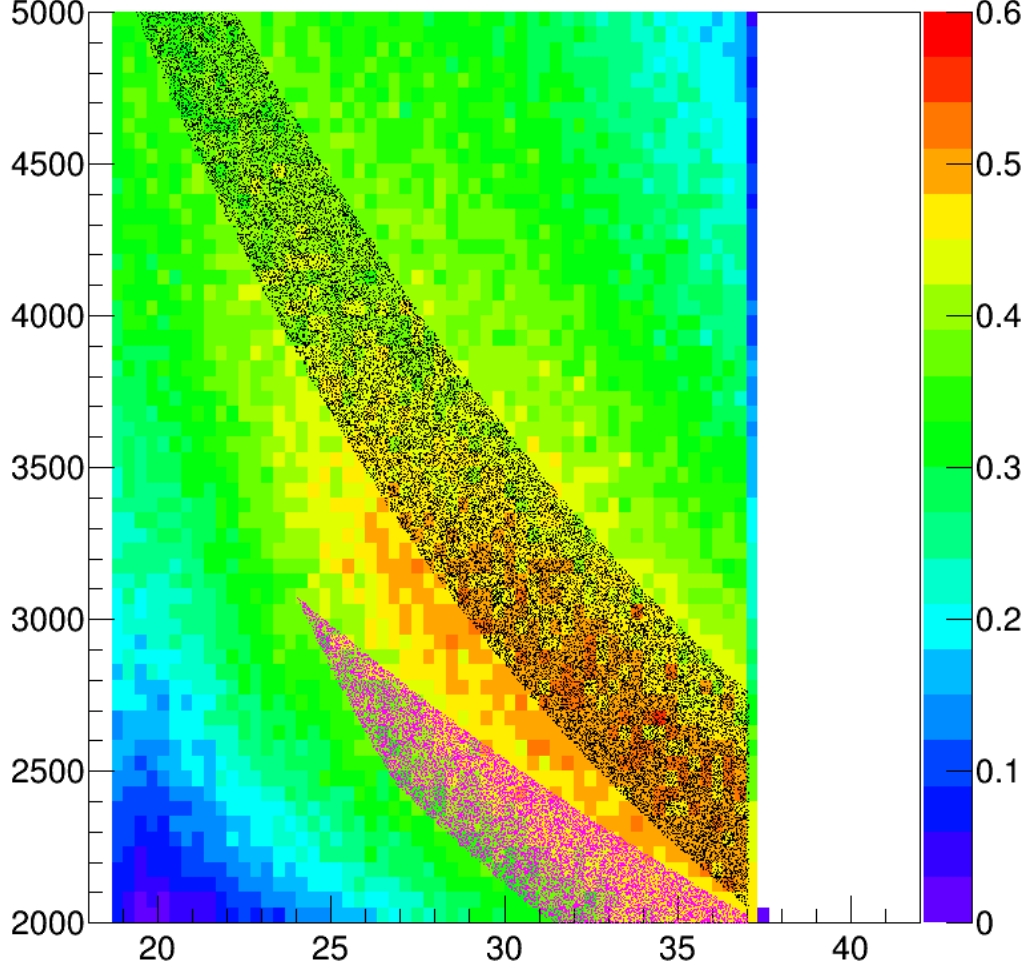


FIG. 24. Color plot: Acceptance as function of p (MeV/c) vs. θ_p (degrees) for electrons produced at target center and traversing Kryptonite More1 baffles with standard geometry except that inner rings are removed. Points: p vs. θ_p for electrons scattered from target center with $p > 2$ GeV/c and $W^2 > 4$ GeV² after traversing Kryptonite More1 baffles. Magenta points are for 6 GeV beam with $Q^2 > 3.5$ GeV/c² and $x_{bj} > 0.45$; black points are for 11 GeV beam with $Q^2 > 6$ GeV/c² and $x_{bj} > 0.55$.

of the first plate's slit were kept approximately fixed, and the other edges were adjusted to conform to the electron tracks that pass our kinematics cuts and get past these defining edges. A significant modification to note is that in the first two plates, the inner rings and small radius constrictions are removed. (Inner rings are used on the other nine plates.) These are here designated "CLEO2" baffles, denoting their being tuned to the CLEO field and distinguishing them from the old CLEO baffles.

Figure 36 is similar to Fig. 22, but the CLEO2 baffles are used; additionally, these electrons are from vertices throughout the target (rather than just the five positions used previously). Note the reduction in the gaps along the slit edges.

Upstream vertex

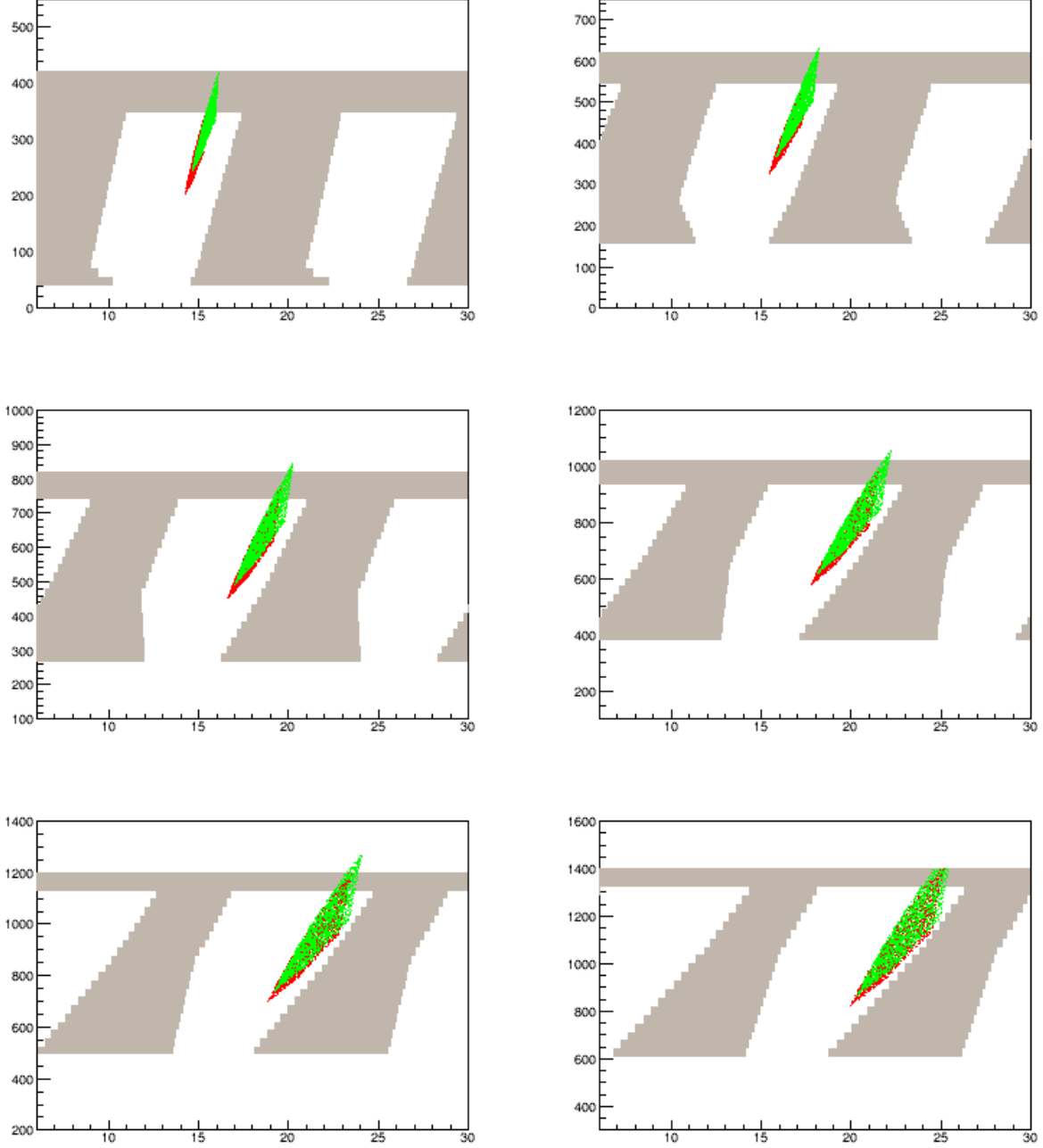


FIG. 25. Positions of electron tracks for $E_{beam} = 6.6$ GeV with $p > 2$ GeV/c, $\phi_p = 12^\circ$, $x_{Bj} > 0.45$, $W^2 > 4$ GeV², $Q^2 > 3.5$ GeV², and vertex at the upstream end of the target for each of the odd numbered baffle plates. Red (green) points are at z corresponding to the upstream (downstream) face of each plate. Baffles were not present in the simulation but their shapes are drawn for reference.

Mid/upstream vertex

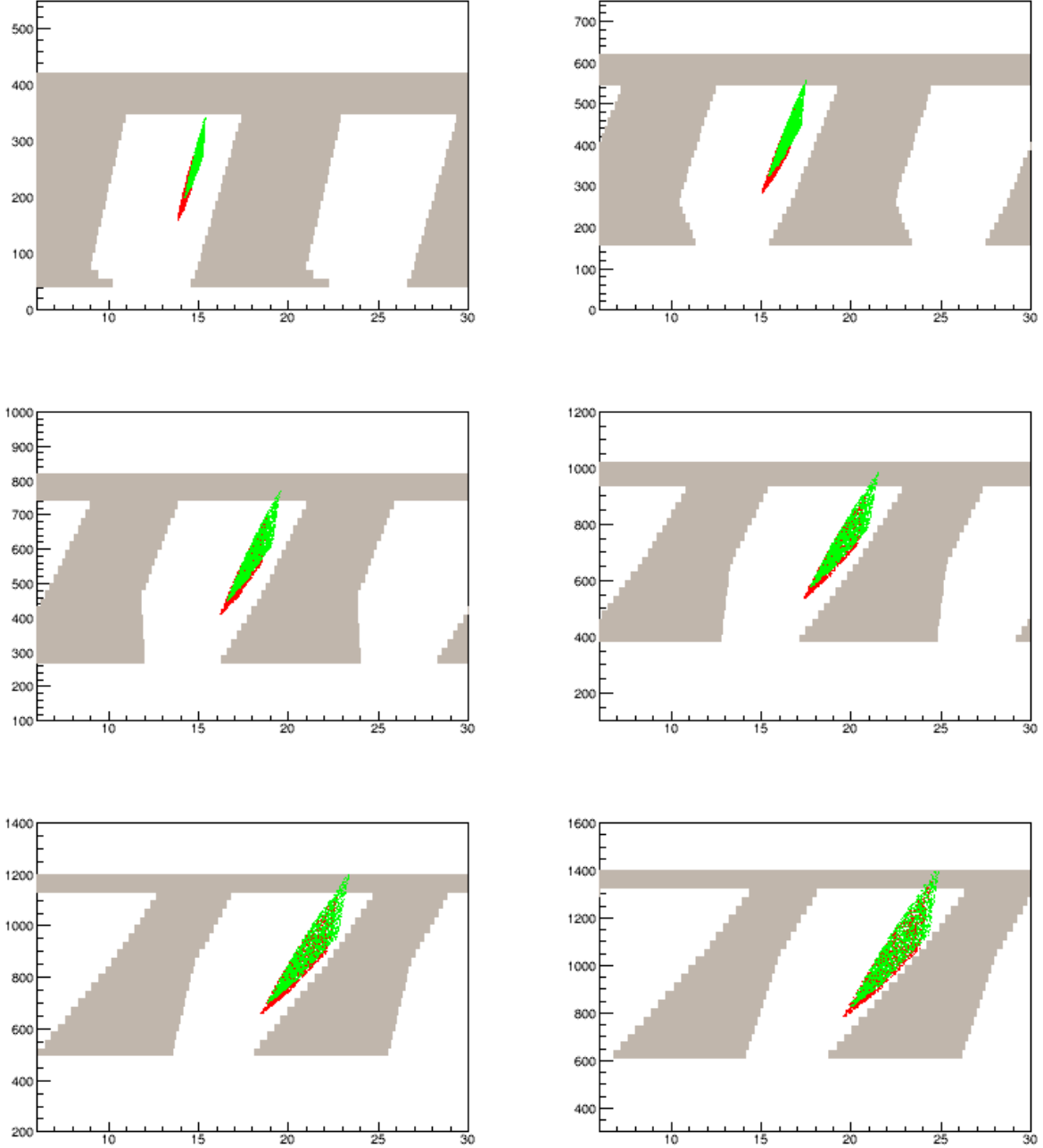


FIG. 26. Positions of electron tracks for $E_{beam} = 6.6$ GeV with $p > 2$ GeV/c, $\phi_p = 12^\circ$, $x_{Bj} > 0.45$, $W^2 > 4$ GeV², $Q^2 > 3.5$ GeV², and vertex halfway the upstream end and center of the target for each of the odd numbered baffle plates. Red (green) points are at z corresponding to the upstream (downstream) face of each plate. Baffles were not present in the simulation but their shapes are drawn for reference.

Middle vertex

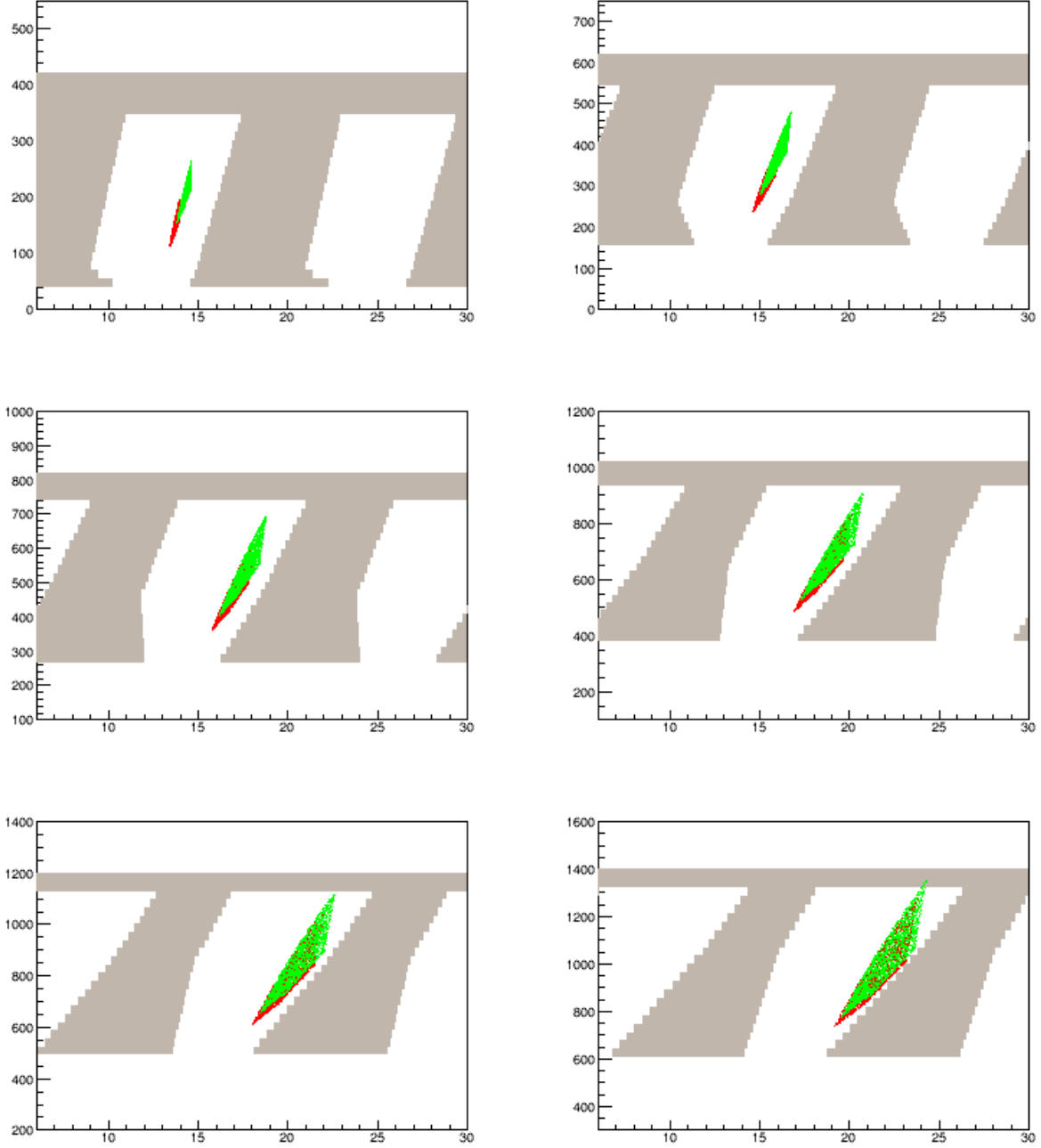


FIG. 27. Positions of electron tracks for $E_{beam} = 6.6$ GeV with $p > 2$ GeV/c, $\phi_p = 12^\circ$, $x_{Bj} > 0.45$, $W^2 > 4$ GeV², $Q^2 > 3.5$ GeV², and vertex at the center of the target for each of the odd numbered baffle plates. Red (green) points are at z corresponding to the upstream (downstream) face of each plate. Baffles were not present in the simulation but their shapes are drawn for reference.

Mid/downstream vertex

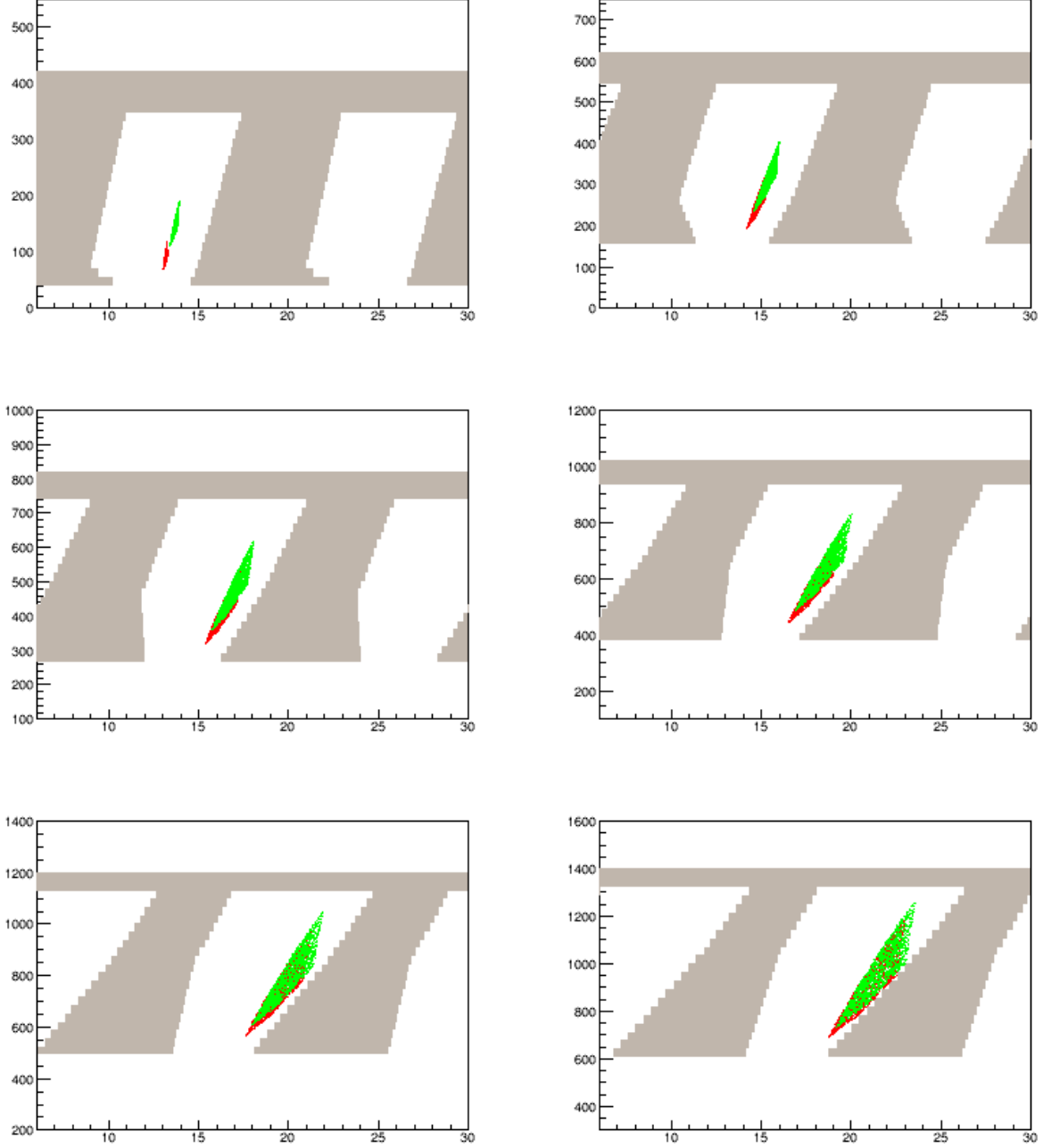


FIG. 28. Positions of electron tracks for $E_{beam} = 6.6$ GeV with $p > 2$ GeV/c, $\phi_p = 12^\circ$, $x_{Bj} > 0.45$, $W^2 > 4$ GeV², $Q^2 > 3.5$ GeV², and vertex halfway between the center and downstream end of the target for each of the odd numbered baffle plates. Red (green) points are at z corresponding to the upstream (downstream) face of each plate. Baffles were not present in the simulation but their shapes are drawn for reference.

Downstream vertex

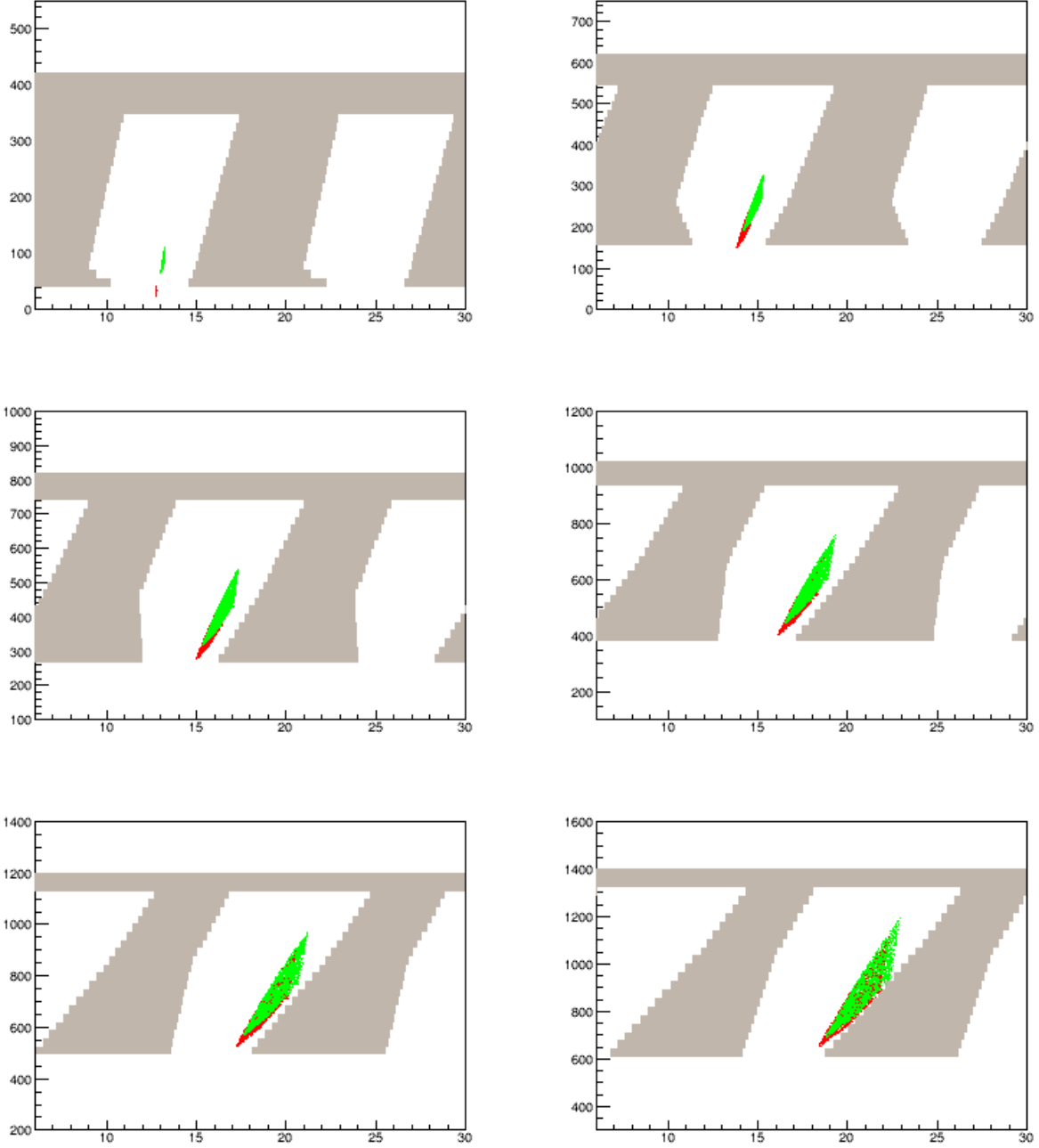


FIG. 29. Positions of electron tracks for $E_{beam} = 6.6$ GeV with $p > 2$ GeV/c, $\phi_p = 12^\circ$, $x_{Bj} > 0.45$, $W^2 > 4$ GeV², $Q^2 > 3.5$ GeV², and vertex at the downstream end of the target for each of the odd numbered baffle plates. Red (green) points are at z corresponding to the upstream (downstream) face of each plate. Baffles were not present in the simulation but their shapes are drawn for reference.

Upstream vertex

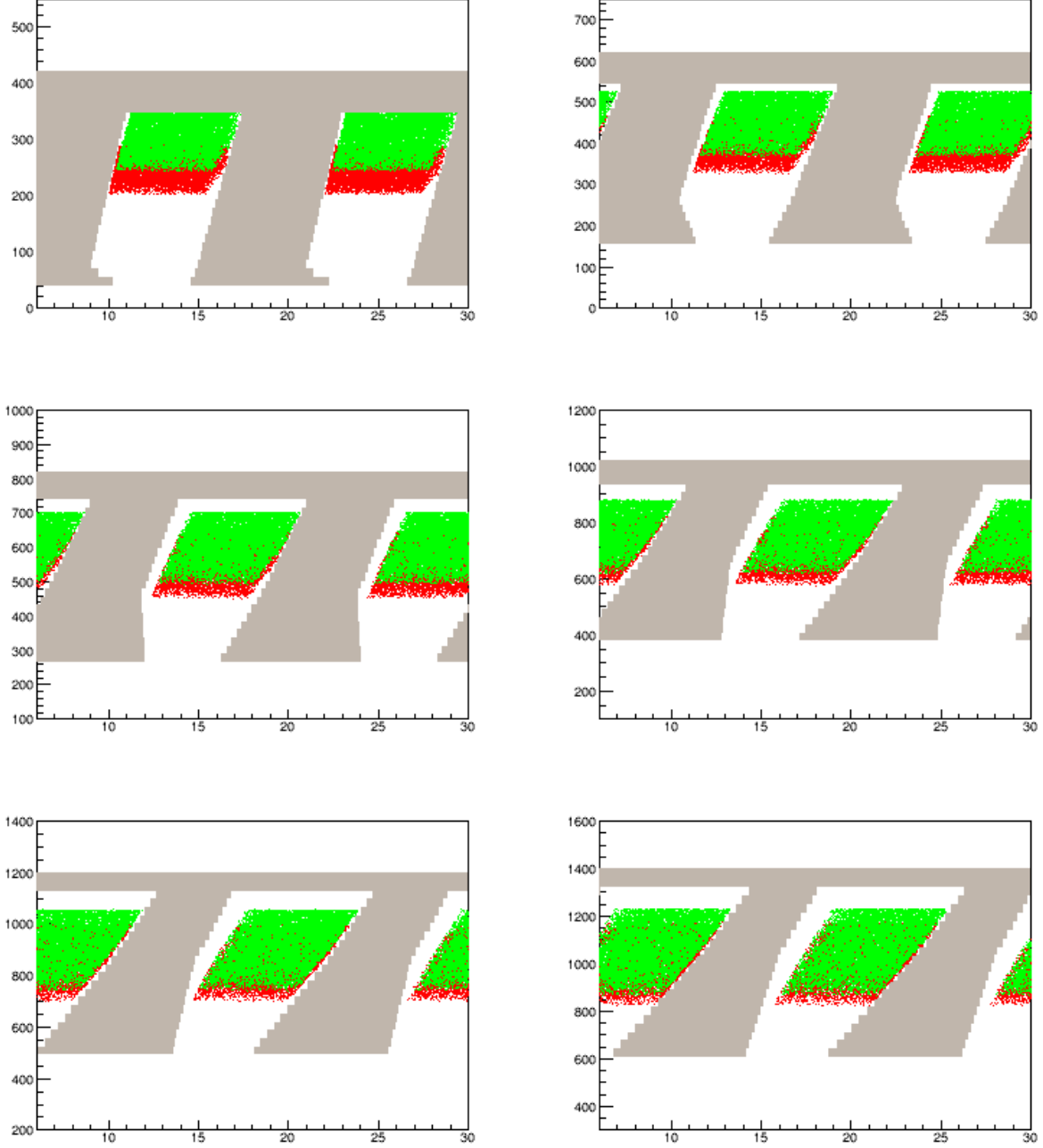


FIG. 30. Positions of electron tracks for $E_{beam} = 6.6$ GeV with $p > 2$ GeV/c, $x_{Bj} > 0.45$, $W^2 > 4$ GeV², $Q^2 > 3.5$ GeV², and vertex at the upstream end of the target for each of the odd numbered baffle plates. Kryptonite More1 baffles (inner ring removed) were present in the simulation, and only electrons which passed through all 11 baffle plates are shown. Red (green) points are at z corresponding to the upstream (downstream) face of each plate.

Mid/upstream vertex

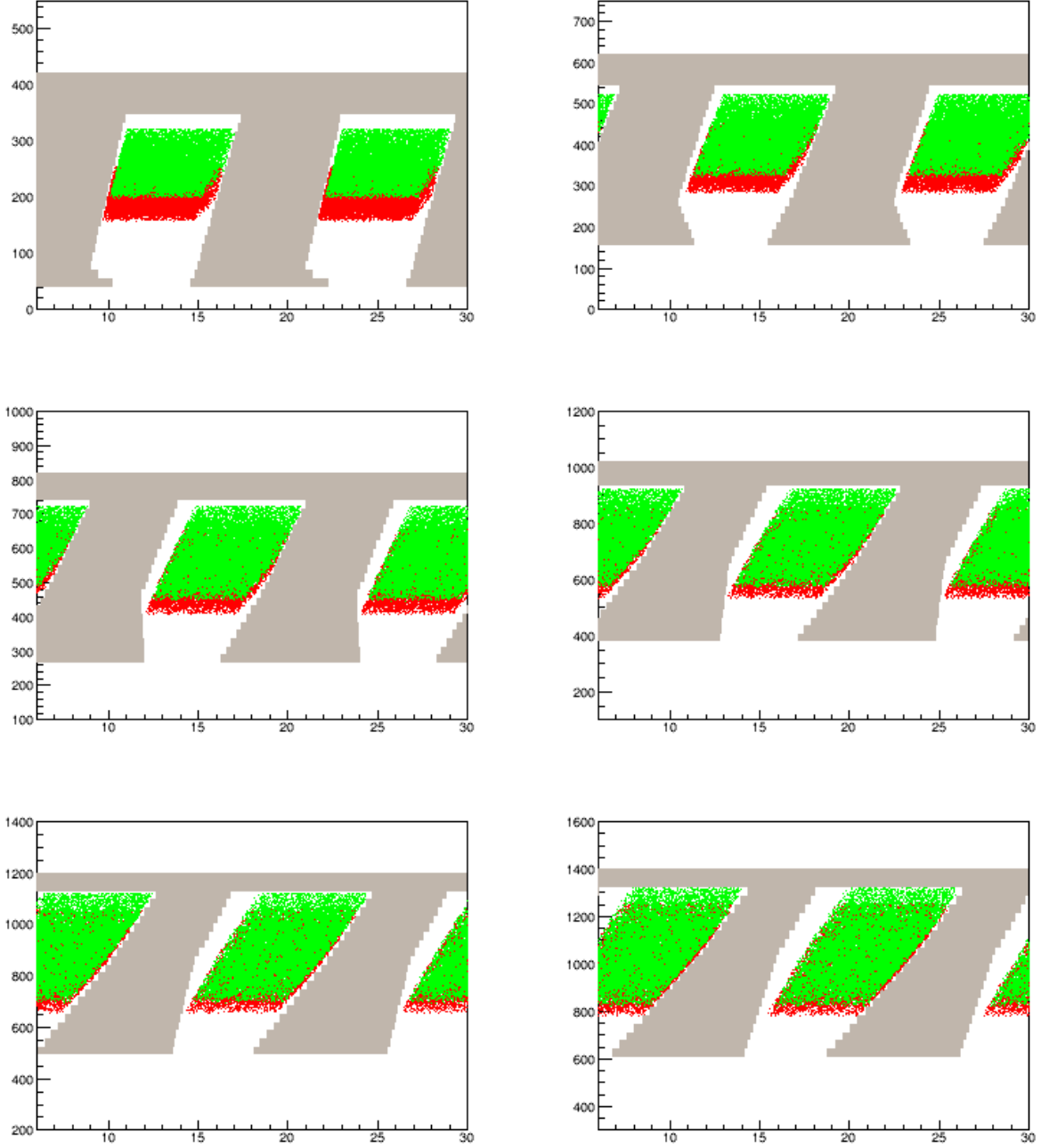


FIG. 31. Positions of electron tracks for $E_{beam} = 6.6$ GeV with $p > 2$ GeV/c, $x_{Bj} > 0.45$, $W^2 > 4$ GeV², $Q^2 > 3.5$ GeV², and vertex halfway the upstream end and center of the target for each of the odd numbered baffle plates. Kryptonite More1 baffles (inner ring removed) were present in the simulation, and only electrons which passed through all 11 baffle plates are shown. Red (green) points are at z corresponding to the upstream (downstream) face of each plate.

Middle vertex

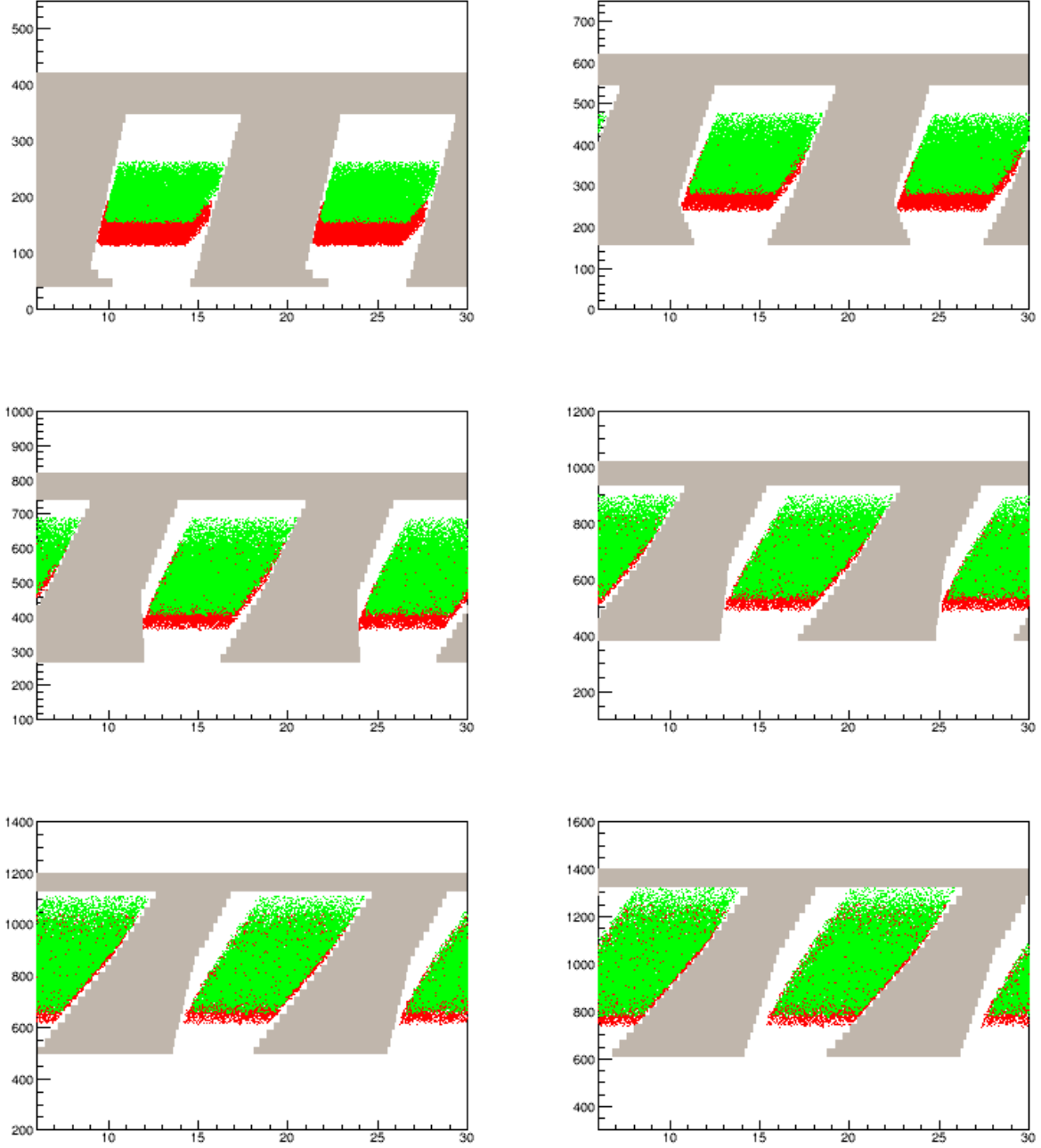


FIG. 32. Positions of electron tracks for $E_{beam} = 6.6$ GeV with $p > 2$ GeV/c, $x_{Bj} > 0.45$, $W^2 > 4$ GeV², $Q^2 > 3.5$ GeV², and vertex at the center of the target for each of the odd numbered baffle plates. Kryptonite More1 baffles (inner ring removed) were present in the simulation, and only electrons which passed through all 11 baffle plates are shown. Red (green) points are at z corresponding to the upstream (downstream) face of each plate.

Mid/downstream vertex

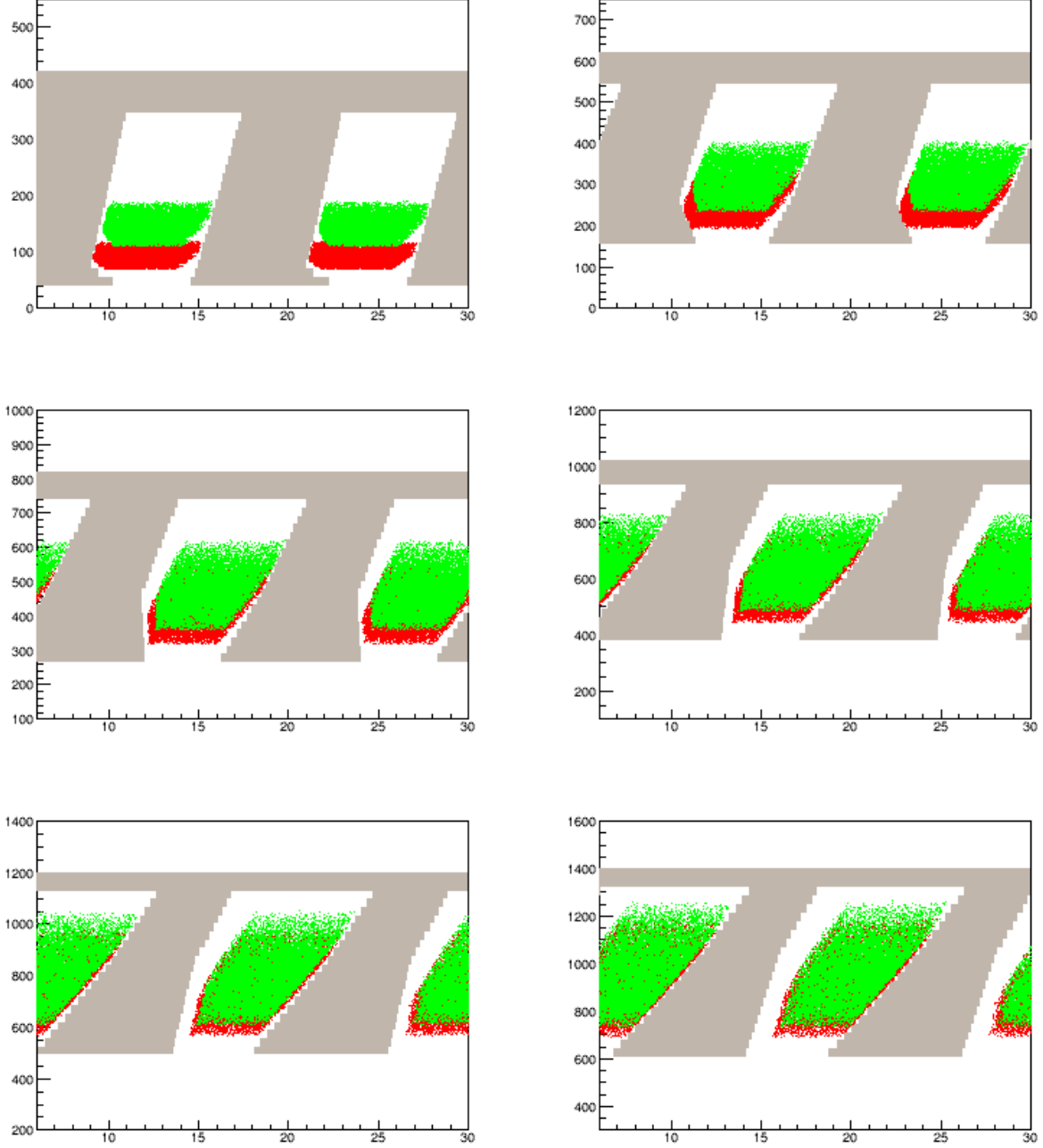


FIG. 33. Positions of electron tracks for $E_{beam} = 6.6$ GeV with $p > 2$ GeV/c, $x_{Bj} > 0.45$, $W^2 > 4$ GeV², $Q^2 > 3.5$ GeV², and vertex halfway between the center and downstream end of the target for each of the odd numbered baffle plates. Kryptonite More1 baffles (inner ring removed) were present in the simulation, and only electrons which passed through all 11 baffle plates are shown. Red (green) points are at z corresponding to the upstream (downstream) face of each plate.

Downstream vertex

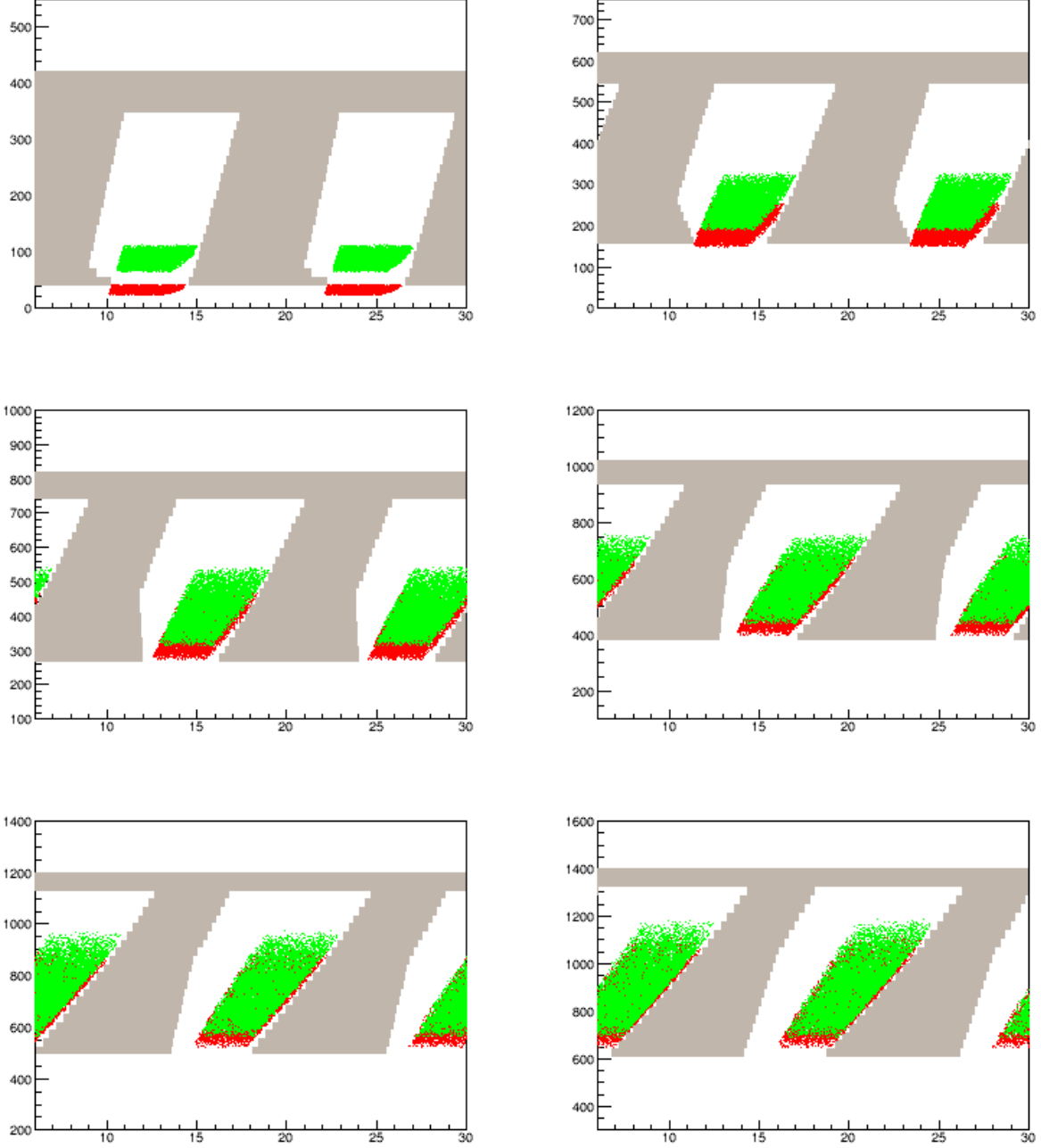


FIG. 34. Positions of electron tracks for $E_{beam} = 6.6$ GeV with $p > 2$ GeV/c, $x_{Bj} > 0.45$, $W^2 > 4$ GeV², $Q^2 > 3.5$ GeV², and vertex at the downstream end of the target for each of the odd numbered baffle plates. Kryptonite More1 baffles (inner ring removed) were present in the simulation, and only electrons which passed through all 11 baffle plates are shown. Red (green) points are at z corresponding to the upstream (downstream) face of each plate.

Baffles comparison

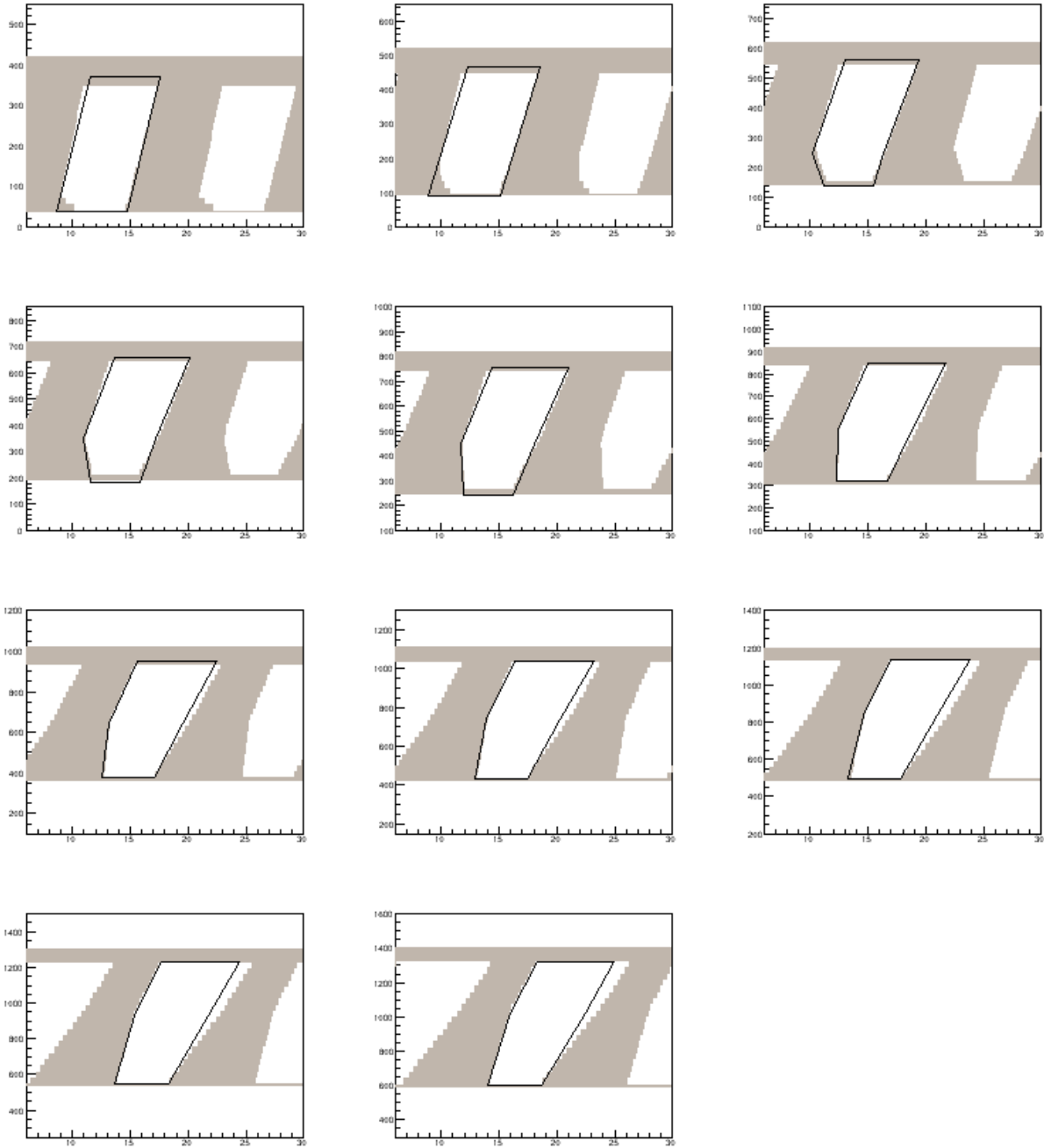


FIG. 35. CLEO2 baffle slit shapes (black lines) superposed on More1 baffle shapes (grey).

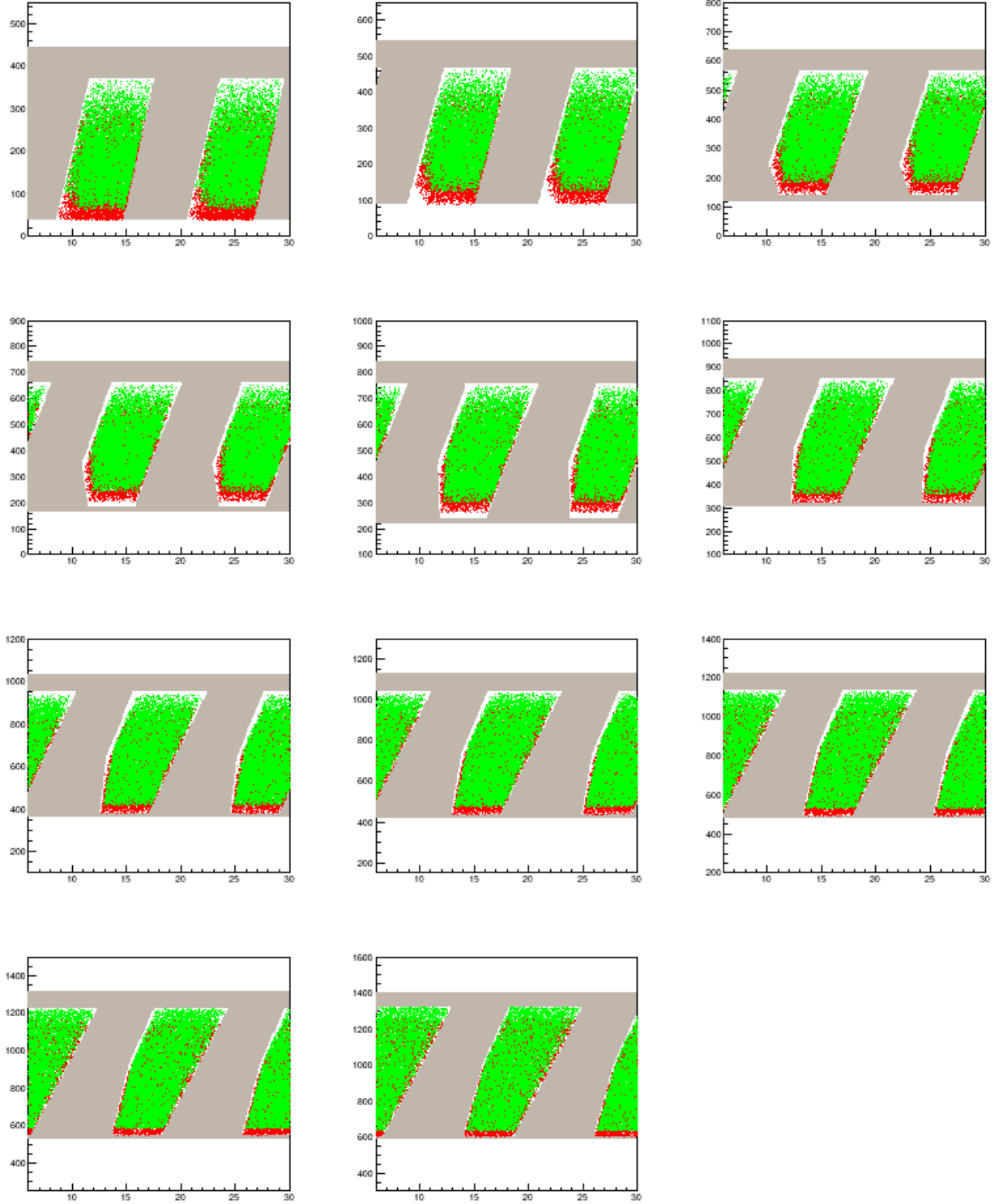


FIG. 36. Positions of electron tracks with $p > 2$ GeV/c, $x_{Bj} > 0.55$, $W^2 > 4$ GeV², $Q^2 > 6$ GeV², and vertex at any position in the target. Kryptonite baffles with the CLEO2 design were present in the simulation, and only electrons which passed through all 11 baffle plates are shown. Red (green) points are at z corresponding to the upstream (downstream) face of each plate.

Figure 37 shows geometrical acceptances as functions of p , θ_p , and z_v for the More1 and CLEO2 baffles. The CLEO2 baffles have similar integrated acceptance, peaking at slightly higher momentum and with significantly lower losses at the target ends. Figures 38 to 40 show color plots of these acceptances versus two variables.

The acceptances for neutrals, shown in Fig. 41, are similar for the More1 and CLEO2 baffles, as expected given that the defining edges are nearly the same. CLEO2 has slightly higher neutrals acceptance from the downstream half of the target.

VII. SUMMARY

The More1 baffles are fairly well matched to our requirements; a few changes give some incremental improvements.

- Opening the slits in the even numbered plates by 0.65° would reduce photon backgrounds by $\sim 20\%$ while increasing charged pions by less than 10% .
- Use of solid tungsten for the baffles probably is impractical and not compellingly motivated. For mechanical reasons we may wish to consider copper baffles with 1° wide lead linings for the slits (and perhaps solid lead for the last baffle), whose performance should be similar to solid lead baffles.
- For the first few upstream plates, replacing the inner rings with extensions of the slits to the minimum radius, if mechanically possible, and eliminating the angular constrictions at small radius recovers acceptance from the downstream end of the target. This is implemented in the CLEO2 baffles.
- Increasing the outer radius of the first few plates improves acceptance from the upstream end of the target. This also is implemented in the CLEO2 baffles.
- Making adjustments to the long slit edges allows a better match the trajectories in the CLEO field. This also is implemented in the CLEO2 baffles.
- Acceptance for straight throughs, at smaller radii along the “hot” edges of the slits, could be reduced by adjusting the slit shape in the last plates, resulting in reduced backgrounds in the GEMs and LGC. This would entail some loss of acceptance for electrons, but it would be small.

While the More1 and CLEO2 baffles are not optimal for 6.6 GeV running, the acceptance is probably still good enough given the rates.

-
- [1] Z. Zhao, “PVDIS baffle material and neutron shielding” (16 Mar 2015)
(http://hallaweb.jlab.org/12GeV/SoLID/download/baffle/talk/solid_baffle_zwzhao_20150316.pdf)
- [2] P. Bosted *et al.*, “Precision Measurement of Parity-violation in Deep Inelastic Scattering Over a Broad Kinematic Range” (15 Dec 2008)

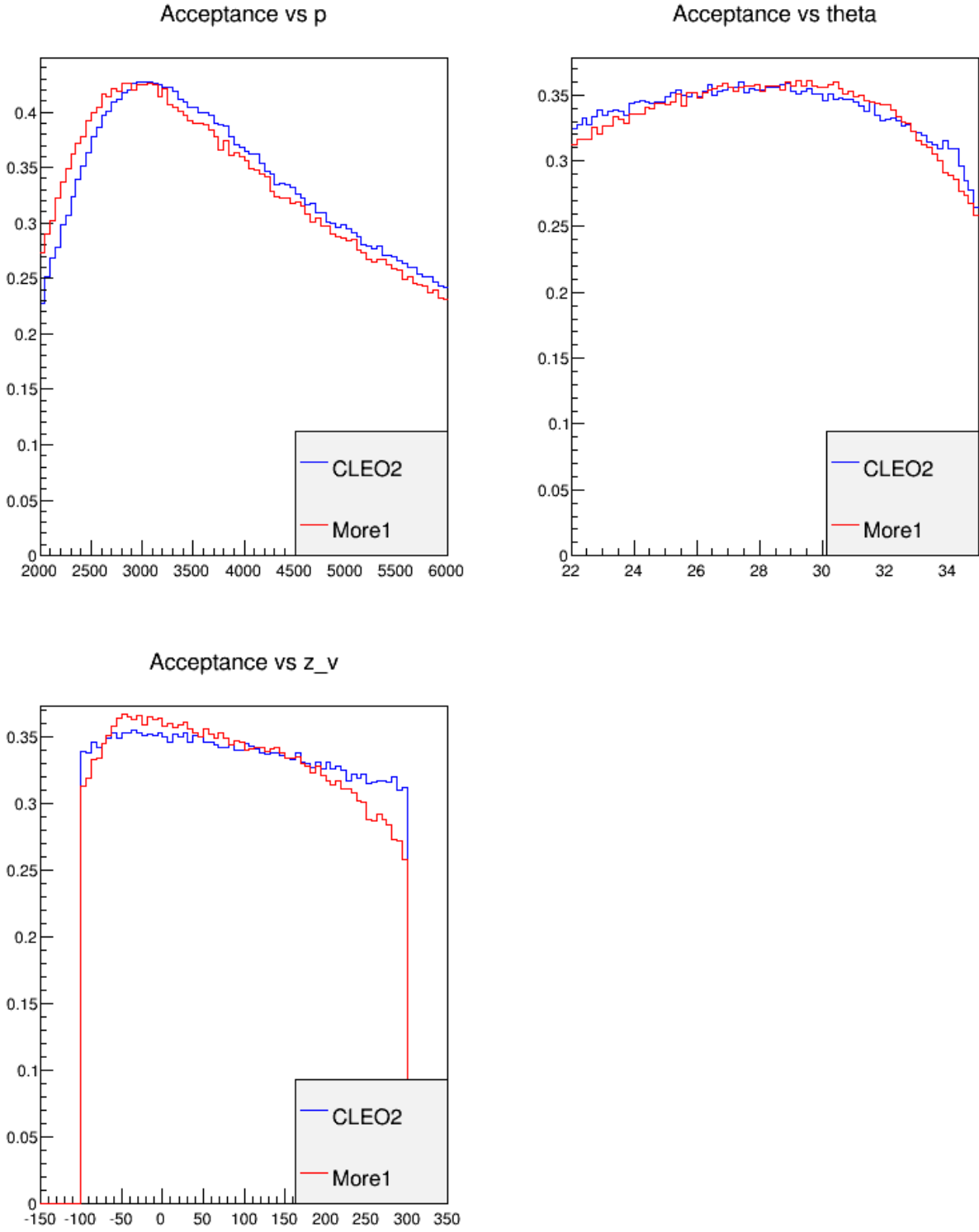


FIG. 37. Geometrical acceptances for electrons passing our kinematics cuts versus p (upper left), θ_p (upper right), and z_v (lower left), shown for More1 baffles (red), and CLEO2 baffles (blue).

Acceptance vs p vs theta

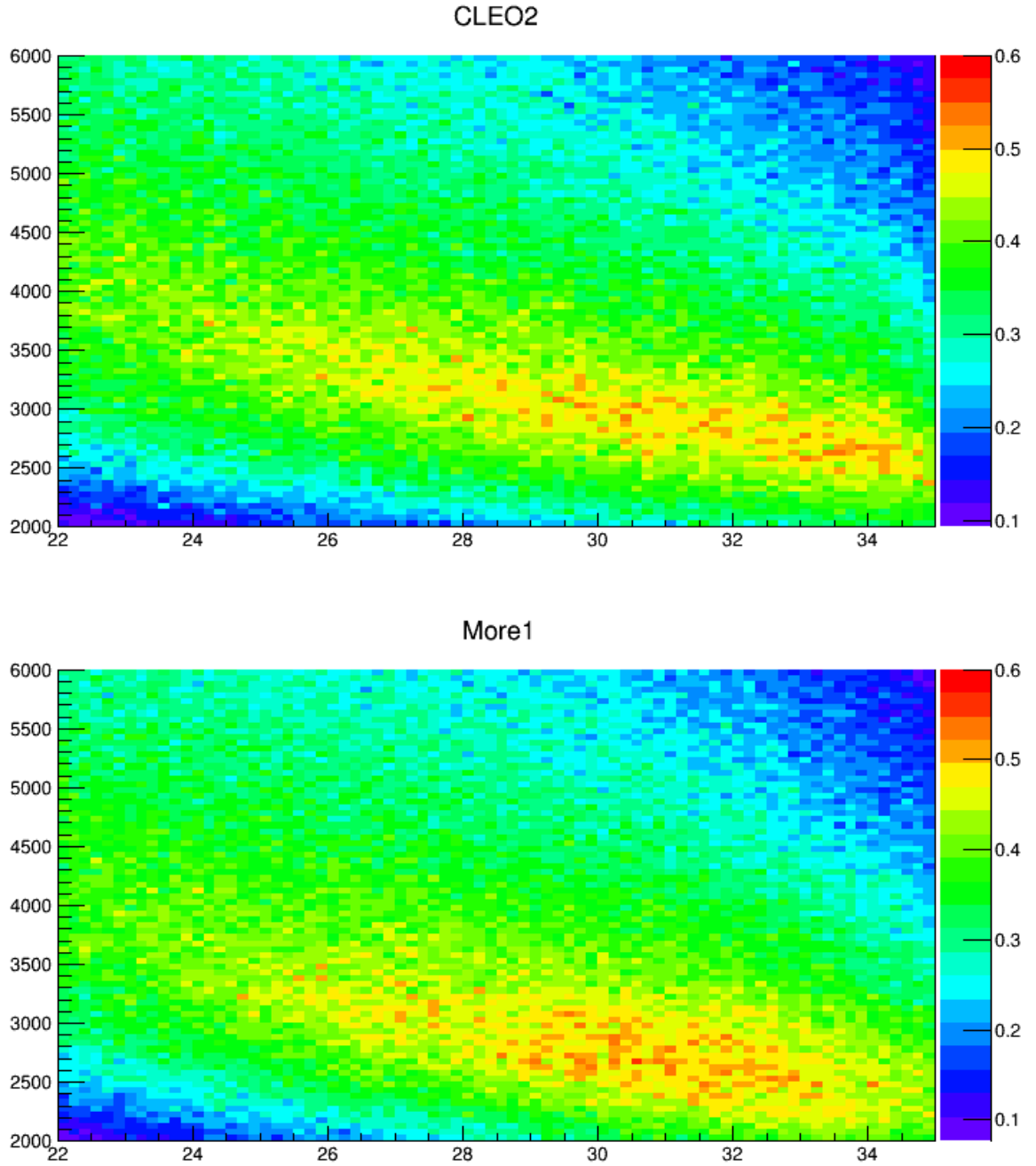


FIG. 38. Geometrical acceptances for electrons passing our kinematics cuts versus p (vertical axis) and θ_p (horizontal axis), shown for CLEO2 baffles (top) and More1 baffles (bottom).

Acceptance vs p vs z_v

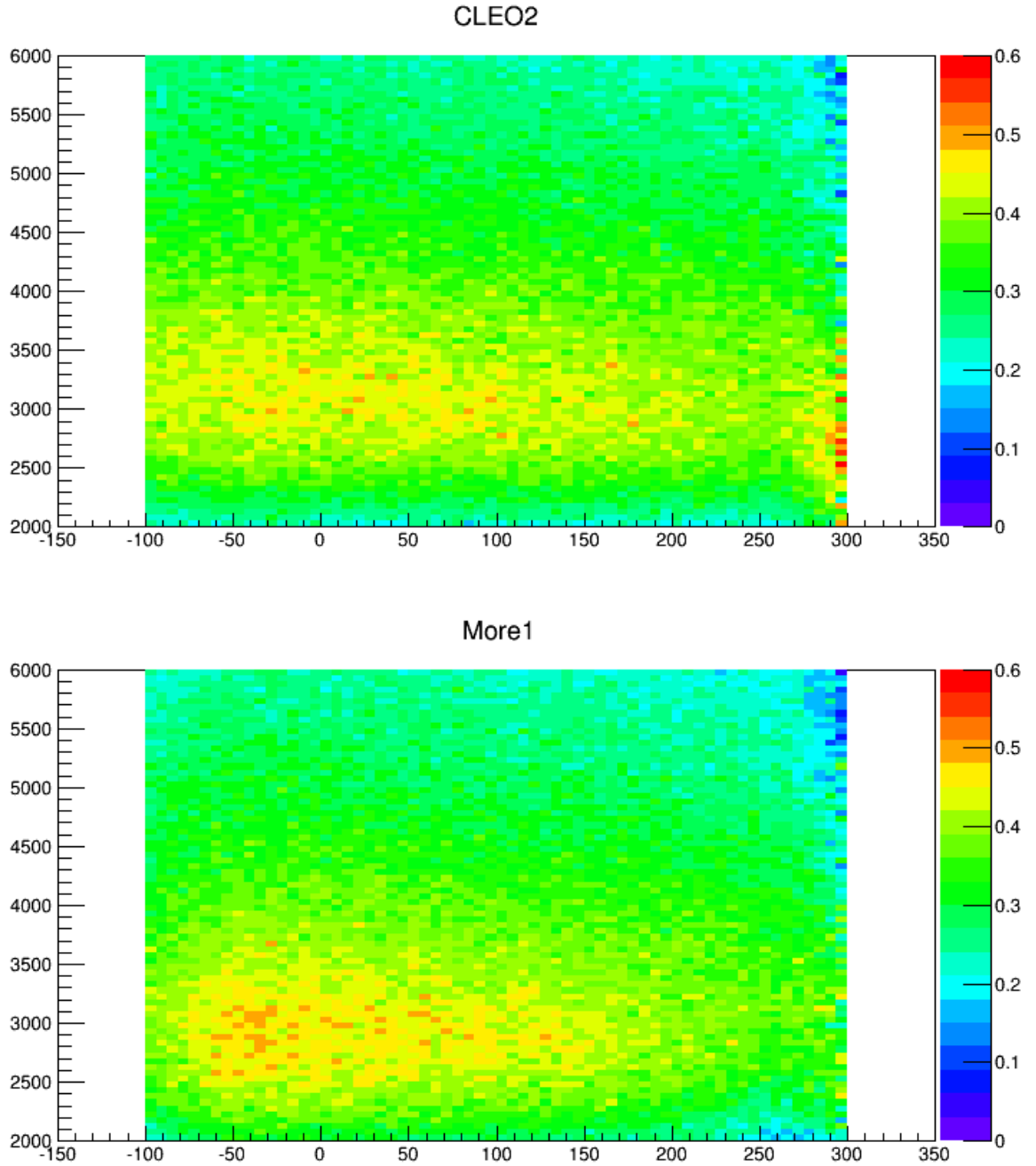


FIG. 39. Geometrical acceptances for electrons passing our kinematics cuts versus p (vertical axis) and z_v (horizontal axis), shown for CLEO2 baffles (top) and More1 baffles (bottom).

Acceptance vs theta vs z_v

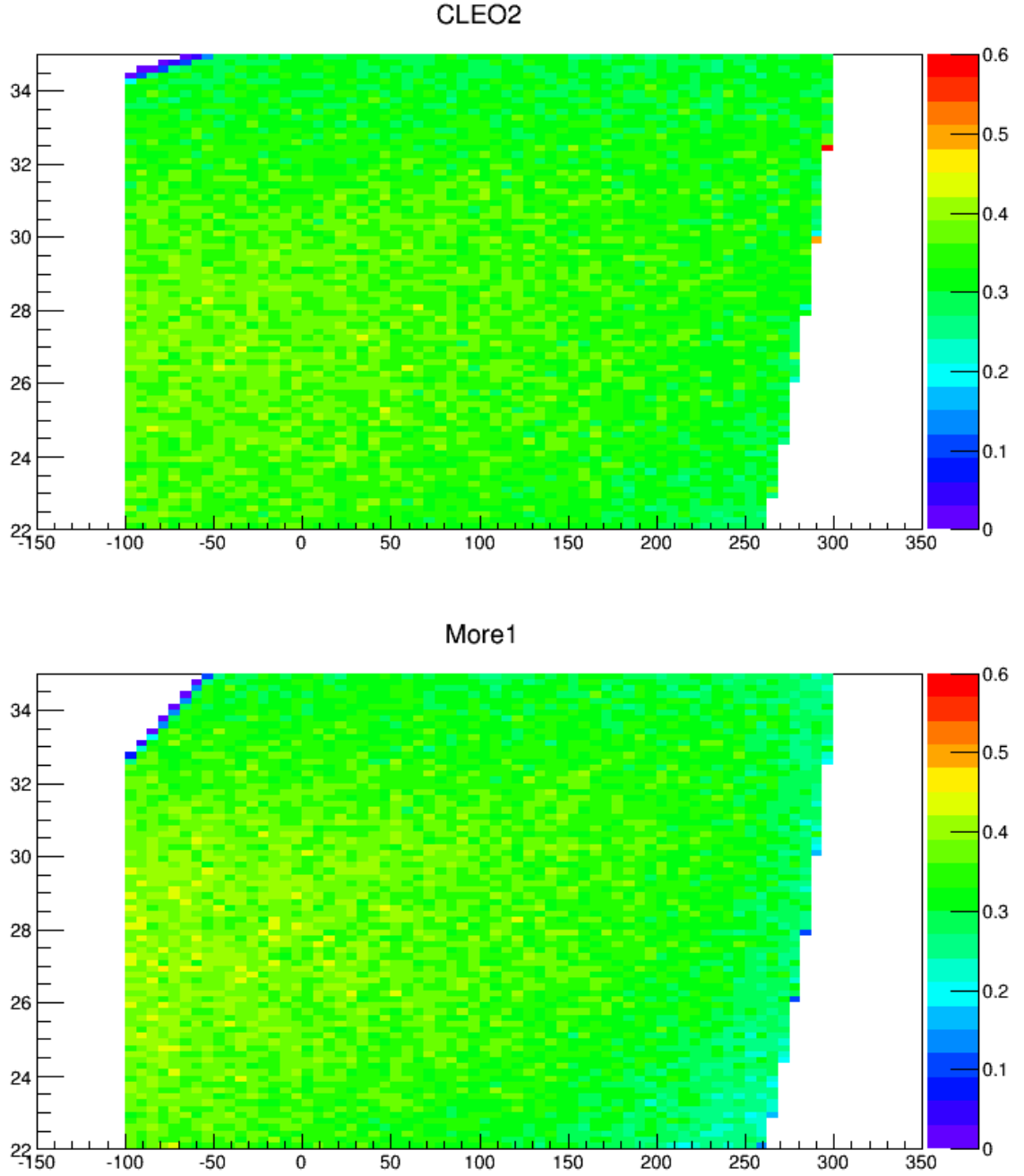


FIG. 40. Geometrical acceptances for electrons passing our kinematics cuts versus θ_p (vertical axis) and z_v (horizontal axis), shown for CLEO2 baffles (top) and More1 baffles (bottom).

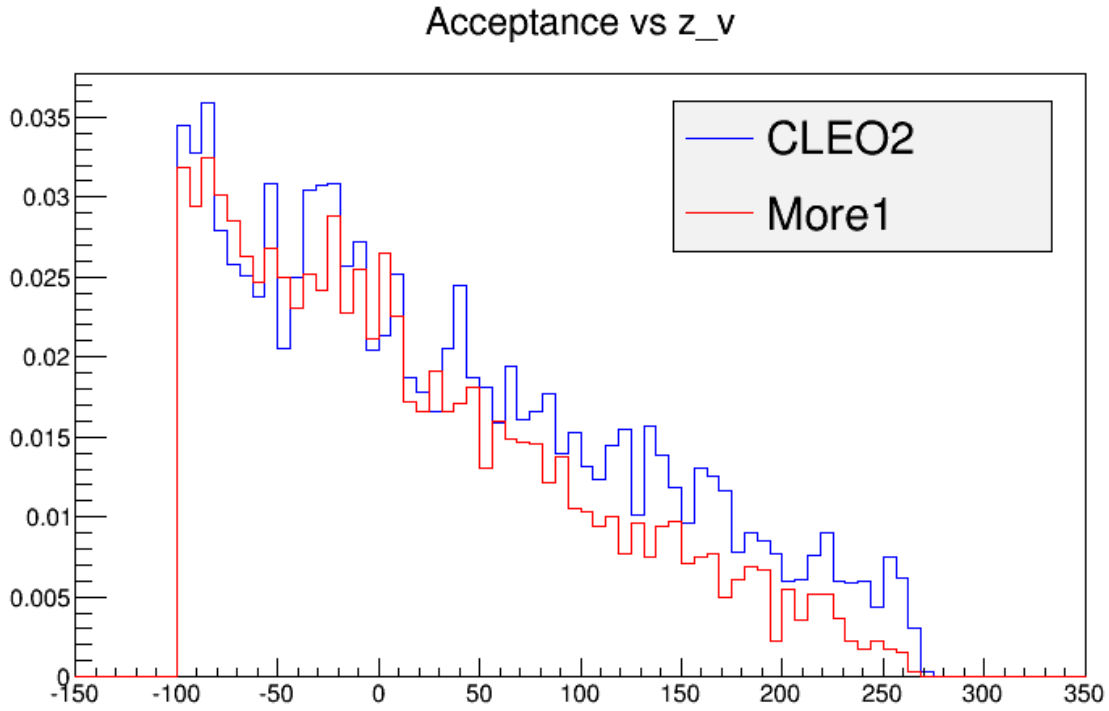
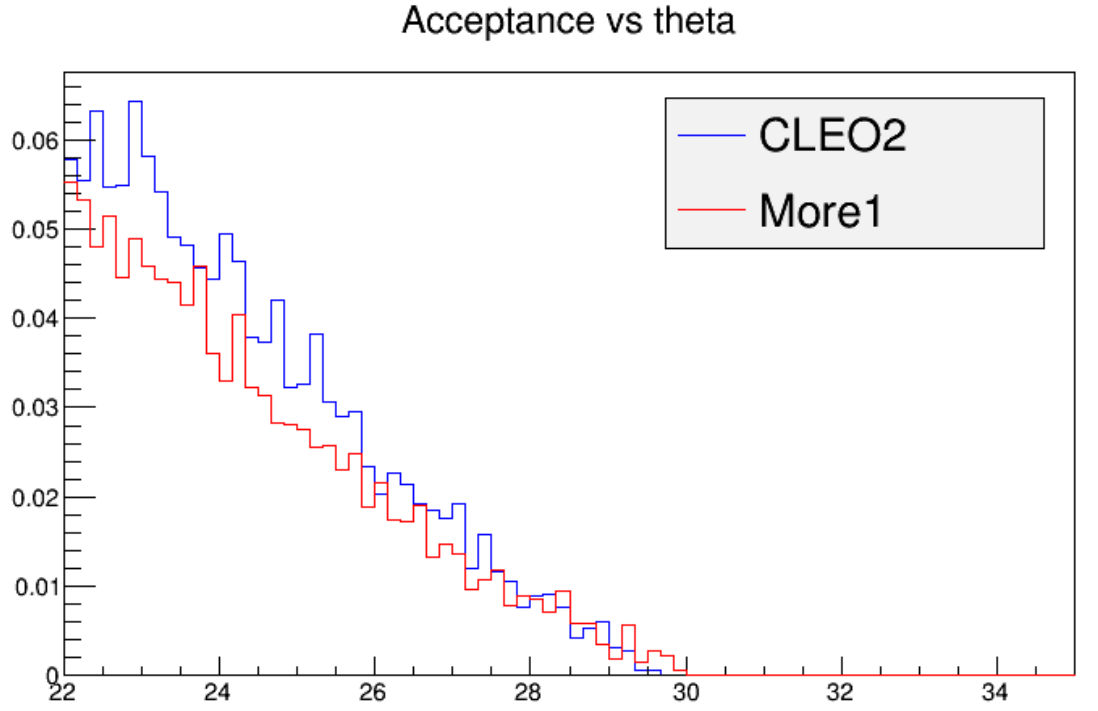


FIG. 41. Geometrical acceptances for photons versus θ_p (top), and z_v (bottom), shown for More1 baffles (red), and CLEO2 baffles (blue).